Universitat Autònoma de Barcelona

Automatic image quantification strategies in clinical nuclear medicine and neuroradiology

Frederic Sampedro Santaló

Programa de Doctorat en Medicina (RD 1393/2007)

Departament de Medicina

Automatic image quantification strategies in clinical nuclear medicine and neuroradiology

Tesis Doctoral presentada per

Frederic Sampedro Santaló

per a obtenir el grau de Doctor per la
Universitat Autònoma de Barcelona

Sota la direcció de:

Prof. Ignasi Carrió Gasset

Dr. Sergio Escalera Guerrero

Dr. Jordi Riba Serrano

A la meva mare i,

especialment,

al meu pare.

"In theory, there is no difference between theory and practice. But, in practice, there is."

Attributed to multiple people. It's so true that it doesn't matter who said it.

Acknowledgements / Agraïments / Agradecimientos

En primer lloc agrair el suport incondicional dels meus pares, que ha estat un pilar fonamental per al desenvolupament d'aquesta tesi.

En segon lloc, agrair al Prof. Ignasi Carrió el fet de donar-me l'oportunitat de realitzar aquesta tesi sota la seva supervisió i, a més, permetre'm "volar sol". Gràcies a ell he pogut organitzar-me el temps amb total llibertat, he pogut compaginar els estudis amb la tesi, i he tingut l'oportunitat de conèixer i col·laborar amb nombrosos grups de recerca de l'Hospital de Sant Pau.

En tercer lloc, agrair al Dr. Sergio Escalera el seu esforç i ajuda en els primers passos d'aquesta tesi, que van ser absolutament claus per endinsar-me amb bon peu en el món de la recerca.

Finalment, el meu sincer agraïment a totes aquelles persones que han col·laborat en fer possible aquesta tesi, especialment als membres del servei de Medicina Nuclear (Dra Anna Domenech, Dra Valle Camacho), de la Unitat de Memòria (Dr Juan Fortea, Eduard Vilaplana), de la Unitat de Trastorns del Moviment (Saül Martínez-Horta, Dr Jaume Kulisevsky), del grup de Neuropsicofarmacologia Humana de l'Hospital de Sant Pau (Dr Jordi Riba) i del departament de matemàtica aplicada i análisis de la UB (Dra Anna Puig).

Index

I. List of publications

1. *Automatic Tumor Volume Segmentation in Whole-Body PET/CT Scans: A Supervised Learning Approach. F. Sampedro, S. Escalera, A. Domenech,I. Carrio. J. Med. Imaging Health Inf. 5, 192-201,2015.*

2. *Obtaining quantitative global tumoral state indicators based on whole-body PET/CT scans: a breast cancer case study. F.Sampedro, A. Domenech, S.Escalera. Nuclear Medicine Communications 35(4),362-371, 2014.*

3. *A computational framework for cancer response assessment based on oncological PET-CT scans. F. Sampedro, S.Escalera, A.Domenech, I.Carrio. Computers in Biology and Medicine 55, 92-99, 2014.*

4. *Deriving global quantitative tumor response parameters from 18F-FDG PET-CT scans in patients with non-Hodgkin's lymphoma. F.Sampedro, A.Domenech, S.Escalera, I.Carrio. Nuclear Medicine Communications 36 (4), 328-333, 2015.*

5. *Computing quantitative indicators of structural renal damage in pediatric DMSA scans. F. Sampedro, A.Domenech, S.Escalera, I.Carrió. Rev Esp Med Nucl Imagen Mol, In Press, 2016.*

6. *APOE-by-sex interactions on brain structure and metabolism in healthy elderly controls. Sampedro F, Vilaplana E, de Leon MJ, Alcolea D, Pegueroles J, Montal V, Carmona-Iragui M, Sala I, Sánchez-Saudinos MB, Antón-Aguirre S, Morenas-Rodríguez E, Camacho V, Falcón C, Pavía J, Ros D, Clarimón J, Blesa R, Lleó A, Fortea J; Alzheimer's Disease Neuroimaging Initiative. Oncotarget. 05 Sep 9;6(9):666-74,2015.*

7. *Non-demented Parkinson's disease patients with apathy show decreased grey matter volume in key executive and reward-related nodes. S.Martínez-Horta & F.Sampedro, J. Pagonabarraga, J. Marín-Lahoz, J.Riba, J.Kulisevsky. Brain Imaging and Behavior, In Press, 2016.*

8. *Telling true from false: Cannabis users show increased susceptibility to false memories.J. Riba, M. Valle & F. Sampedro, A. Rodríguez-Pujadas, S. Martinez-Horta, J. Kulisevsky, A.Rodriguez-Fornells. Molecular Psychiatry 20, 772–777,2015.*

II. Thesis introduction, motivation and background

Digital medical imaging has been one of the revolutions in medicine of the last two decades. Medical specialists currently have available a wide range of imaging modalities that have raised the diagnostic quality and follow-up evaluation of many pathologies.

Most medical images used in clinical practice are visually evaluated by the trained physician in order to detect and characterize the presence of a particular pathology of interest. While in most cases this procedure is assumed to obtain the best accuracy, it has several imitations. First, the diagnostic performance is highly dependent on the physician's expertise. Second, the diagnostic product is generally categorical (i.e. positive/negative/inconclusive) and descriptive, lacking a quantitative modeling of the characteristics underlying a disorder. Finally, some image modalities cannot be directly evaluated visually due to their technical nature (e.g. resting-state cerebral functional magnetic resonance imaging), requiring image-derived quantitative indicators to be properly assessed.

To overcome these limitations and given the increasing computational power of modern technology, the automatic computation of quantitative indicators in medical images that could complement the visual evaluation by the trained physician is emerging as an important research area. Notably, the information from this type of indicators would be, by definition, observer-independent and quantitative.

Therefore, for each medical scenario and image modality of interest, the challenge of designing the best computational image-quantification strategy capable of obtaining new indicators that could improve diagnostic accuracy, prognosis estimation or disease understanding is clearly appealing to the medical community.

The possible incorporation of this type of indicators in healthcare centers would have major advantages at several levels. At the clinical level, if the image-derived quantitative indicators aided in the interpretation of complex radiological patterns by providing relevant observer-independent diagnostic information, they would contribute to a better overall diagnostic accuracy, especially in situations where there is limited physician expertise on this task. At the management level, if the availability of such indicators contributed to accelerate the determination of radiological conclusions, an increase in diagnostic throughput would be obtained, thus providing significant management and economic benefits to the health institution.

III. Objectives

The main objective of this thesis is to provide scientific contributions to the field of automatic medical image quantification for clinical or research applications. Among the large number of medical imaging modalities and clinical contexts, this thesis will only focus on the computation of quantitative indicators from the following image modalities: FDG-PET scans (whole-body and cerebral), renal DMSA-scans, T1-weighted magnetic resonance imaging (cerebral), and cerebral event-related functional magnetic resonance imaging. Details about these image modalities are given throughout this section.

The indicators computed from these images were designed to contribute to application-specific scenarios in several medical domains, including tumor burden evaluation, structural kidney damage quantification, neurodegenerative disease characterization and drug-induced brain activation analysis.

In this section, each of these image quantification contexts is described and the original research papers derived from them are mentioned, whereas the next section will summarize its main results and discussions.

The first automatic image quantification scenario of this thesis was related to tumor burden characterization in oncological whole-body FDG-PET scans. This type of scan is a valuable nuclear medicine test where a whole-body image of the subject is obtained, showing the uptake distribution of a glucose-analog radioactive tracer. The diagnostic power of this imaging technique relies on the fact that elevated tracer uptake (a proxy for high metabolic activity) in certain anatomical locations may indicate the presence of a tumor.

In this first image analysis context, the main objective was to obtain a numerical indicator from FDG-PET scans that was able to model underlying tumor properties (i.e. volume, metabolic uptake and spread) in a quantitative and expert-independent manner (Fig.1).

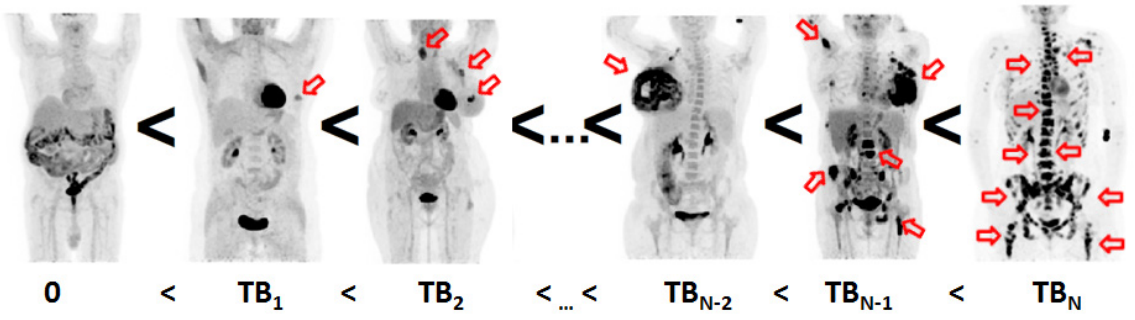

Fig.1 First scenario: automatic computation of an efficient image-derived tumor burden indicator (TBI) in whole-body FDG-PET scans to model quantitatively the spectrum of tumor states in the population. Red arrows indicate the presence of tumor volume in that anatomical region.

From the technical point of view, a key step needed to automatically compute this type of indicator is that a computer algorithm should be able to detect and segment the tumor

volume of *any* given whole-body FDG-PET scan. Given the substantial variability of the human anatomy and physiological tracer uptake of the population in this context, this poses *per se* a major computational problem.

Therefore, the first contribution (article [1]) sought to apply state-of-the-art machine learning and computer vision algorithms to automatically detect and segment tumor volume in this type of scans. Then, having the tumor volume segmented from the images either by using automatic or expert-guided segmentation techniques, the scenario of computing accurate numerical indicators that would be able to model the underlying tumor characteristics was addressed in article [2]. Both of these works used a cohort of breast cancer patients where novel quantitative indicators could contribute to obtain image-derived prognostic indicators of the disease.

In the same image modality context but addressing a different clinical scenario, the computation of quantitative indicators modeling the tumor response in time from a pair of pre- and post- treatment FDG-PET scans was addressed; both at the technical and clinical levels (articles [3] and [4]). In this case, a cohort of non-Hodgkin lymphoma patients with a pair of time-consecutive FDG-PET scans was used to derive new indicators to quantify the tumor progression or response.

The second image quantification context sought to detect and characterize structural renal damage in DMSA scans. This type of scan is also a nuclear medicine image where the radiotracer used shows the distribution of the DMSA molecule within the kidneys. This distribution is of particular diagnostic interest since healthy kidney tissue would tend to show high tracer uptake, whereas damaged kidney regions would show less or no tracer uptake.

The automatic computation of numerical indicators in this type of image (Fig.2) led to the contribution presented in article [5], where a pediatric cohort of patients with structural kidney damage was used to obtain image-derived quantitative indicators of the underlying renal pathology.

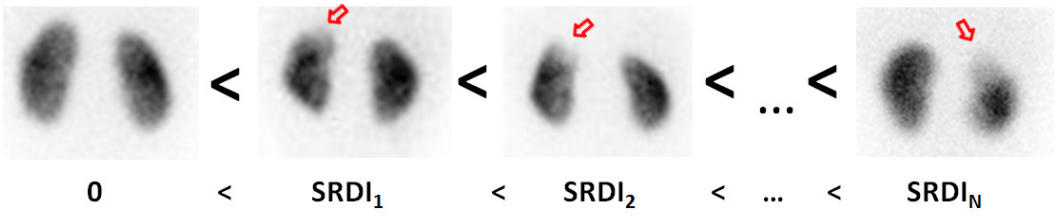

Fig.2 Second scenario: automatic computation of an image-derived efficient structural renal damage indicator (SRDI) in DMSA scans to model quantitatively the underlying pathology. Red arrows indicate structural renal damage in those kidney areas.

The third image analysis scenario aimed to quantify the metabolic activity from cerebral FDG-PET scans (described above) in a set of key brain areas related to dementia such as the temporal lobe (Fig.3). In this case, the relationship between such imaging indicators, the APOE genotype (the best-known genetic risk factor for Alzheimer's disease) and gender in healthy controls was investigated in article [6].

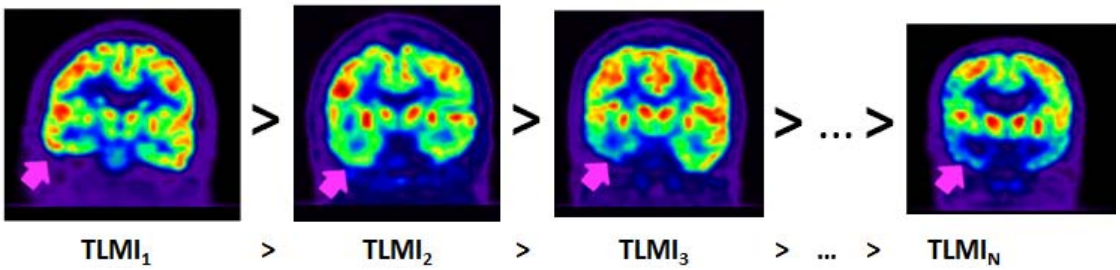

Fig 3 Third scenario: automatic computation of an efficient temporal lobe metabolism indicator (TLMI) in cerebral FDG-PET scans to model quantitatively the underlying pathophysiology of Alzheimer's disease. Pink arrows illustrate the metabolic activity of a region in the left temporal lobe.

The fourth and fifth image quantification contexts were performed on cerebral T1-weighted magnetic resonance maging (MRI) scans. By applying a combination of magnetic fields and radio frequency pulses to the brain, tissues with different properties generate different signals that can be detected and processed, obtaining a structural brain image where gray matter, white matter, and cerebrospinal fluid can be distinguished.

The amount and distribution of gray matter in the brain is key to correct brain functioning. An accurate measure of the integrity of gray matter within the cerebral cortex (responsible for cognition and memory among other important functions) is cortical thickness, defined by the distance between the white matter and pial surfaces. For subcortical brain structures such as the basal ganglia, gray matter volume can be computed by direct segmentation of the volumetric image.

Cortical atrophy (i.e. reduction of cortical thickness) is one of the hallmarks of Alzheimer's disease, whereas alterations in the gray matter volume of the basal ganglia are associated with movement disorders (Fig. 4).

The work described in article [6] also addressed the quantification of cortical thickness in key areas of the cerebral cortex to also analyze the influence of APOE and gender on brain atrophy associated with the Alzheimer's disease.

Quantification of gray matter volume in a specific region of the basal ganglia known as the nucleus accumbens (a key node of the brain's reward circuit) was performed in Parkinson's disease patients with apathy. This aimed to provide a neuroanatomical basis for this behavioral manifestation, which plays an important role as a marker of disease progression (article [7]).

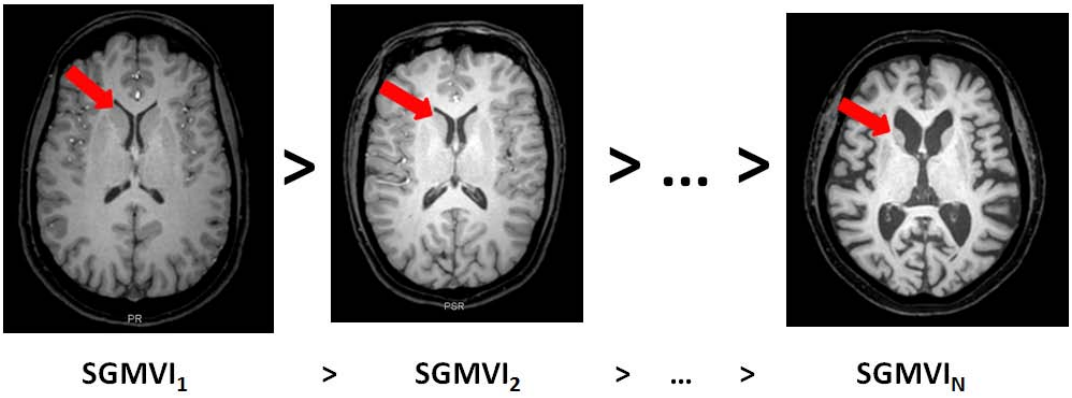

Fig. 4. Fifth scenario: automatic computation of a striatal gray matter volume indicator (SGMVI) in T1-MRI images to model quantitatively the underlying pathophysiology of Parkinson's disease. Red arrows illustrate the gray matter volume of a portion of the left caudate nucleus.

The sixth and last image analysis scenario was related to the quantification of functional magnetic resonance (fMRI) images. Neuronal activation requires energy, and therefore the vascular system provides nutrients and oxygen to those neurons that have increased activation. This regional change of the vascular content and flow in the regions where there is a high neuronal activity can be detected using Blood-oxygen-level dependent (BOLD) MRI signal.

By acquiring a set of BOLD fMRI images for a period of time, the brain activity during specific events can be recorded. If a particular task is performed during the acquisition, the activation of a particular brain region of interest related to that specific task can be computed (Fig.5).

In article [8], cortical and hippocampal activation during a false memory rejection task was quantified from the BOLD images in a set of cannabis users and healthy controls. Areas of differential activation between groups were identified. Activity in these brain regions were correlated with individual values of lifetime cannabis use. Results identified novel memory impairments in users and increased our understanding of the deleterious impact of cannabis on cognition.

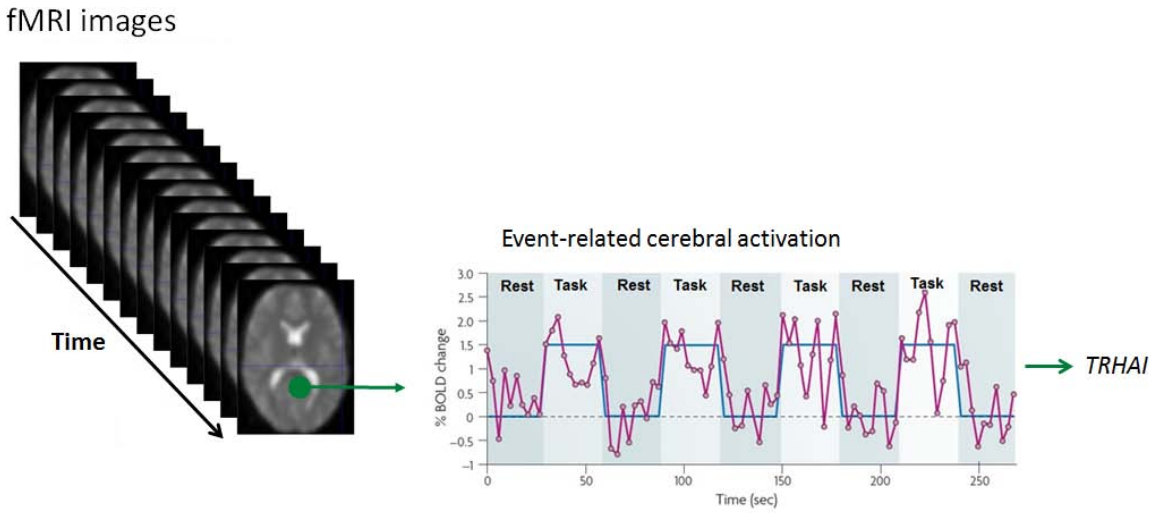

Fig. 5. Sixth scenario: automatic computation of a task-related hippocampal activation indicator (TRHAI) from event-related fMRI images to quantitatively model the possible memory alterations in cannabis users.

IV. Summary of the contribution's results and discussion

In this section, a brief summary of the main results and discussion of each of the works introduced in the previous section is presented.

Automatic Tumor Volume Segmentation in Whole-Body PET/CT Scans: A Supervised Learning Approach. F. Sampedro, S. Escalera, A. Domenech,I. Carrio. J. Med. Imaging Health Inf. 5, 192-201,2015.

In this work the application-specific problem of automatic detection and segmentation of tumor volume in whole-body FDG-PET/CT scans was addressed.

The visual inspection by the medical specialist of whole-body FDG-PET/CT scans is a valuable diagnostic tool in oncological scenarios. Furthermore, the possibility of quantifying a set of tumor properties (such as its total volume or metabolic uptake) using expert-guided segmentation tools offers additional clinical value. However, this expert-guided segmentation process is highly time-consuming and expert-dependent. This work addressed the need to automate this task and proposed a computational system to do so.

By applying state-of-the-art machine learning techniques (Multiscale-Stacked Sequential Learning), an automatic FDG-PET tumor segmentation system was obtained. Machine learning techniques are a type of artificial intelligence algorithms that learn how to accomplish a particular task if they are provided with a set of training examples. In this case, expert-guided tumor segmentations of 100 breast cancer FDG-PET scans were used to let the system learn a set of segmentation rules.

The segmentation results of the automatic system achieved, at the pixel/voxel level, on average 49% sensitivity, 99% specificity and 39% Jaccard Overlap Index (a measure of comparison of automatic vs. expert-derived segmentation results). Furthermore, the total tumor volume of the breast cancer scans was computed from both expert-guided and automatic segmentation outputs, showing a correlation of 73%.

Conceptually, these results show that the obtained automatic segmentation system successfully detected and segmented only very clear and reasonably-sized tumor regions within the scans. They also suggest that even though the automatic segmentation accuracy at the pixel-level may not be equivalent to that obtained by the manual segmentation performed by a trained physician, at the global indicator level (such as the whole body total tumor volume), the automatically-computed indicators would have potential diagnostic value within the clinical environment.

Obtaining quantitative global tumoral state indicators based on whole-body PET/CT scans: a breast cancer case study. F.Sampedro, A. Domenech, S.Escalera. Nuclear Medicine Communications 35(4),362-371, 2014.

In this work, the need to find a set of quantitative indicators derived from the image analysis of whole body FDG-PET/CT scans aiming to model properly the global oncological state of the patient was addressed.

A set of 100 breast cancer FDG-PET/CT scans were classified according to their global oncological state following visual evaluation by a consensus of nuclear medicine physicians. A set of quantitative indicators derived from the tumor segmentation of the images was then computed, both using completely automatic and expert-guided approaches. The performance of these indicators at modeling the patient's underlying oncological state as classified by the expert's visual inspection was measured.

The performance results of the commonly used indicators in clinical practice including whole-body metabolic tumor volume (WBMTV), maximum/mean metabolic activity of the tumor (SUVmax/SUVmean), and a combination of both (Total Lesion Glycolysis) achieved performances ranging from 49% to 79% (in a measure of correlation with the expert's classification).

None of these indicators take into account the spread of the tumor across the patient's body (i.e. the number of anatomical structures where the tumor is present). This work proposed to include that information into the computation of the indicators, obtaining new indicators that improved performance from 80 to 87%. These results were obtained using expert-guided tumor segmentations. Using a completely automatic approach, the best performance result was 64%.

Taken together, this work contributed to show that image-derived FDG-PET global quantitative indicators can prove useful in clinical nuclear medicine and oncological scenarios. Furthermore, the incorporation of tumor spread measures in the computation of such indicators improved its performance at modeling the underlying oncological state. Finally, a substantial performance difference between the expert-guided and the completely automatic computation of the indicators was observed, suggesting that there is room for improvement in this research line.

A computational framework for cancer response assessment based on oncological PET-CT scans. F. Sampedro, S.Escalera, A.Domenech, I.Carrio. Computers in Biology and Medicine 55, 92-99, 2014.

In the following two works, a different clinical scenario within the whole-body PET-CT image analysis context was addressed: the quantification of oncological state changes over time.

This first contribution focused exclusively on the design and implementation of a computational framework aimed to correctly identify the most common clinical cancer evolution scenarios (i.e. progression, partial response, total response, mixed response, and relapse) from a pair of time consecutive PET-CT scans of the patient. This task, visually performed by nuclear medicine physicians in clinical practice (suffering from the common expert-dependence and qualitative diagnostic product limitations), poses a challenging problem within a computational environment.

Performance results at predicting the cancer evolution scenario in a set of 100 non-Hodgkin lymphoma (NHL) patients achieved up to 90% of accuracy when using expert-guided image-derived tumor segmentations and 70% accuracy when using a completely automatic approach. These results suggest that computing a set of image-derived quantitative indicators of cancer dynamics is only reasonable if expert-derived tumor segmentation information is available.

Deriving global quantitative tumor response parameters from 18F-FDG PET-CT scans in patients with non-Hodgkin's lymphoma. F.Sampedro, A.Domenech, S.Escalera, I.Carrio. Nuclear Medicine Communications 36 (4), 328-333, 2015.

Based on the results of the previous study, this work focused on the actual computation of image-derived quantitative indicators designed to model the magnitude of cancer response or progression conditions.

A set of 89 pairs of time consecutive PET-CT scans presenting NHL were classified by a consensus of nuclear medicine physicians into progressions, partial responses, mixed responses, complete responses, and relapses. The cases of each group were ordered by magnitude following visual analysis. Thereafter, a set of quantitative indicators designed to model the cancer evolution magnitude within each group were computed using expert-guided and automatic image-processing techniques. Performance evaluation of the proposed indicators was measured by a correlation analysis with the expert-based visual analysis.

The set of proposed indicators achieved the following correlation results in each group with respect to the expert-based visual analysis: 80.2% in progressions, 77.1% in partial responses, 68.3% in mixed responses, 88.5% in complete responses, and 100% in relapses. In the progression and mixed response groups, the proposed indicators outperformed the common indicators used in clinical practice (i.e. changes in WBMTV, SUVmax, SUVmean, and total lesion glycolysis) by more than 40%. These results were

obtained using expert-guided tumor segmentations. In this scenario, the automatic approach obtained very poor performance results (<30%).

These results show that the computation of global indicators of NHL response using PET-CT imaging techniques offers a strong correlation with the associated expert-based visual analysis, motivating the future incorporation of such quantitative and highly observer-independent indicators in oncological decision making or treatment response evaluation scenarios. However, a robust automatic approach to the computation of such indicators is still to be obtained.

Computing quantitative indicators of structural renal damage in pediatric DMSA scans. Rev Esp Med Nucl Imagen Mol, In Press, 2016.

The aim of this work was to propose, implement and validate a computational DMSA quantification framework for the computation of image-derived indicators that seek to model the underlying structural renal damage in a quantitative and observer-independent manner.

With this objective in mind, a set of image-derived quantitative indicators based on the relative lesion's size, intensity and histogram distribution was computed from a set of 16 pediatric DMSA-positive scans and 16 matched controls, using both expert-guided and automatic approaches. A correlation analysis was conducted to investigate the association of these indicators with other clinical data of interest in this scenario, including C-reactive protein (CRP), leukocyte count, vesicouretral reflux, fever, relative perfusion, and the presence of renal sequelae in a 6-month follow-up DMSA scan.

A fully automatic lesion detection and segmentation system successfully classified DMSA-positive scans from negative scans (AUC=0.92, sensitivity=81% and specificity =94%). The image-computed relative lesion size correlated with the presence of fever and CRP levels ($p<0.05$), and a measure derived from the histogram distribution of the lesion gave significant performance results in detecting permanent renal damage (AUC=0.86, sensitivity=100% and specificity=75%).

These results suggest that the proposal and implementation for the first time of a computational framework to quantify structural renal damage from DMSA scans shows promising potential to complement visual diagnosis and non-imaging indicators.

APOE-by-sex interactions on brain structure and metabolism in healthy elderly controls. Sampedro F, Vilaplana E, de Leon MJ, Alcolea D, Pegueroles J, Montal V, Carmona-Iragui M, Sala I, Sánchez-Saudinos MB, Antón-Aguirre S, Morenas-Rodríguez E, Camacho V, Falcón C, Pavía J, Ros D, Clarimón J, Blesa R, Lleó A, Fortea J; Alzheimer's Disease Neuroimaging Initiative. Oncotarget. 05 Sep 9;6(9):666-74.

In this work, the objective was to obtain image-derived quantitative indicators of hypometabolism and atrophy in some key areas of the brain related to Alzheimer's disease (AD), and relate them to a set of well-known risk factors of the disease.

In particular, the computation of glucose uptake and cortical thickness indicators within the brain's temporal lobe in a particular population of interest was addressed in order to understand a specific phenomenon observed at the clinical level related to the APOE4 genotype.

The APOE4 variant is the largest known genetic risk factor for late-onset sporadic AD. Epidemiologically, it has been shown that the APOE4 effect on Alzheimer Disease risk is stronger in women than in men. However, the underlying neural mechanisms of this observation had not been established. In this study, the APOE-by-sex interaction on brain metabolism, brain structure, and other indicators of interest such as cerebro-spinal fluid (CSF) was addressed.

This analysis was conducted in a sample of 328 healthy elderly controls from the Alzheimer's Disease NeuroImaging initiative database. Focusing on the brain metabolism and structure interaction results, sex stratification showed that female APOE4 carriers presented widespread brain hypometabolism and atrophy with respect to non-carriers. In contrast, APOE4 male carriers showed only a small region of hypometabolism and no atrophy with respect to non-carriers. This significant hypometabolic and atrophy pattern difference was especially prominent in the temporal lobe, a key brain region involved in AD ($p<0.001$).

These results suggest that the impact of APOE4 on brain metabolism and structure is strongly modified by sex, providing a biologically plausible explanation to the clinical observations. This finding should be taken into consideration in the interpretation of image-derived metabolic indicators commonly used in the clinical management of AD.

Non-demented Parkinson's disease patients with apathy show decreased grey matter volume in key executive and reward-related nodes. Brain Imaging and Behavior, In Press, 2016

In this work, the gray matter volume (GMV) quantification of a set of Parkinson's disease (PD) T1-MRI images contributed to understanding the neuroanatomical basis of apathy in this disease.

For this purpose, two groups of 18 PD patients with available T1-MRI scans were identified. Both groups were equivalent in terms of sociodemographic characteristics,

disease stage and treatment type. The groups only differed in the manifestation of apathy.

The quantification of GMV in cortical and subcortical structures showed that the apathetic group had reduced GMV in the nucleus accumbens ($p<0.005$), a key node of the brain's reward circuit, possibly explaining the motivational deficit observed in apathetic patients. Apathetic patients also had reduced GMV in regions involved in executive functions such as the orbitofrontal cortex ($p<0.005$). Moreover, the patients' GMV at those regions correlated with their cognitive performance ($p<0.001$).

These results suggest apathy as a marker of more widespread brain degeneration in Parkinson's disease.

Telling true from false: Cannabis users show increased susceptibility to false memories. J. Riba, M. Valle, F. Sampedro, A. Rodríguez-Pujadas, S. Martinez-Horta, J. Kulisevsky, A.Rodriguez-Fornells. Molecular Psychiatry (2015) 20, 772–777.

In this work the computation of event-related brain activation indicators was addressed. In particular, a group of 16 heavy cannabis users (which abstained from the drug at least 4 weeks prior to this study) and their matched controls performed a memory task within a functional magnetic resonance imaging (fMRI) scan.

The task performed within the fMRI station implemented a well-established method, the Deese-Roediger-McDermott paradigm, used to experimentally induce memory illusions or "false memories". In this task, "lure" stimuli have to be adequately identified and rejected by the participant.

Notably, cannabis users performed significantly poorer than the controls in this task: the number of incorrectly identified lure stimuli was higher in the cannabis-using group ($p<0.01$).

In order to obtain the neural correlates of this observation, quantitative indicators of brain activation during the task were computed in specific brain areas. Cannabis users showed widespread cortical hypoactivation following lure stimuli rejection. The brain areas involved were located in the frontal and parietal cortices and in the medial temporal lobe in a region including the hippocampus. These areas are known to be involved in executive control, attention and memory processes.

The fact that the hippocampal activation was significantly lower in the cannabis users ($p<0.001$) indicate a possible memory alteration. Importantly, the hippocampal activation in this group was inversely correlated with the lifetime amount of cannabis used by the subjects ($p<0.01$), further supporting the association of the brain's hypoactivation and the drug use.

These findings suggest that cannabis users have an increased susceptibility to memory distortions even when abstinent and drug-free, suggesting a long-lasting compromise of memory and cognitive control mechanisms involved in reality monitoring.

V. General conclusions and final remarks

This thesis presents a set of contributions to the field of automatic and quantitative analysis of digital medical images in nuclear medicine and neuroradiology. This expanding field aims to provide better diagnostic accuracy and help to detect subtle anatomical, physiological or pathological changes in clinical groups that may contribute to our understanding of disease etiologies.

On one hand, this work contributed to increasing the diagnostic potential of breast cancer and non-Hodgkin lymphoma FDG-PET scans through the design and computation of a set of novel image-derived quantitative indicators of tumor burden. In addition, quantitative analysis of pediatric DMSA scans helped to develop new indicators of structural renal damage.

On the other hand, the application-specific quantification of cerebral FDG-PET and T1-MRI scans contributed to the understanding of the pathogenesis of Alzheimer's and Parkinson's diseases, whereas the quantification of event-related fMRI images identified a novel memory deficit associated to cannabis use.

Taken together, these contributions illustrate the potential value of the design and implementation of ad-hoc automated quantification strategies of medical images. The availability of new imaging modalities sparks the search for optimal image-derived quantitative indicators that model each particular clinical context of interest. Such indicators can be used either to complement visual diagnosis or to aid in the comprehensive characterization of the underlying pathology.

VI. Original research papers

Automatic Tumor Volume Segmentation in Whole-Body PET/CT Scans: A Supervised Learning Approach. F. Sampedro, S. Escalera, A. Domenech,I. Carrio. J. Med. Imaging Health Inf. 5, 192-201,2015.

Obtaining quantitative global tumoral state indicators based on whole-body PET/CT scans: a breast cancer case study. F.Sampedro, A. Domenech, S.Escalera. Nuclear Medicine Communications 35(4),362-371, 2014.

A computational framework for cancer response assessment based on oncological PET-CT scans. F. Sampedro, S.Escalera, A.Domenech, I.Carrio. Computers in Biology and Medicine 55, 92-99, 2014.

Deriving global quantitative tumor response parameters from 18F-FDG PET-CT scans in patients with non-Hodgkin's lymphoma. F.Sampedro, A.Domenech, S.Escalera, I.Carrio. Nuclear Medicine Communications 36 (4), 328-333, 2015.

Computing quantitative indicators of structural renal damage in pediatric DMSA scans. F. Sampedro, A.Domenech, S.Escalera, I.Carrió. Rev Esp Med Nucl Imagen Mol, In Press, 2016.

Non-demented Parkinson's disease patients with apathy show decreased grey matter volume in key executive and reward-related nodes. S.Martínez-Horta & F.Sampedro, J. Pagonabarraga, J. Marín-Lahoz, J.Riba, J.Kulisevsky. Brain Imaging and Behavior, In Press, 2016.

APOE-by-sex interactions on brain structure and metabolism in healthy elderly controls

Frederic Sampedro[1,2,3,*], Eduard Vilaplana[1,2,*], Mony J de Leon[4], Daniel Alcolea[1,2], Jordi Pegueroles[1,2], Victor Montal[1,2], María Carmona-Iragui[1,2], Isabel Sala[1,2], María-Belén Sánchez-Saudinos[1,2], Sofía Antón-Aguirre[1,2], Estrella Morenas-Rodríguez[1,2], Valle Camacho[3], Carles Falcón[5,7], Javier Pavía[6,7], Domènec Ros[5,7], Jordi Clarimón[1,2], Rafael Blesa[1,2], Alberto Lleó[1,2], Juan Fortea[1,2] for the Alzheimer's Disease Neuroimaging Initiative[**]

[1]Memory Unit, Department of Neurology, Hospital de la Santa Creu i Sant Pau- Biomedical Research Institute Sant Pau- Universitat Autònoma de Barcelona, Barcelona, Spain

[2]Centro de Investigación Biomédica en Red de Enfermedades Neurodegenerativas. CIBERNED, Madrid, Spain

[3]Nuclear Medicine Department, Hospital de la Santa Creu i Sant Pau- Biomedical Research Institute Sant Pau- Universitat Autònoma de Barcelona, Barcelona, Spain

[4]New York University School of Medicine, New York, NY, USA

[5]Unitat de Biofísica i Bioenginyeria, Departament de Ciències Fisiològiques I, Facultat de Medicina, Universitat de Barcelona – IDIBAPS, Barcelona, Spain

[6]Nuclear Medicine Department. Hospital Clínic de Barcelona, Barcelona, Spain

[7]Biomedical Research Networking Center in Bioengineering, Biomaterials and Nanomedicine - CIBER-BBN, Barcelona, Spain

[*]These authors have contributed equally to this work

[**]Data used in preparation of this article were obtained from the Alzheimer's Disease Neuroimaging Initiative (ADNI) database (adni.loni.usc.edu). As such, the investigators within the ADNI contributed to the design and implementation of ADNI and/or provided data but did not participate in analysis or writing of this report. A complete listing of ADNI investigators can be found at: http://adni.loni.usc.edu/wp-content/uploads/how_to_apply/ADNI_Acknowledgement_List.pdf.

Correspondence to:
Juan Fortea, **e-mail:** jfortea@santpau.cat

Keywords: *Gerotarget, Alzheimer's disease, aging, APOE, MRI, PET-FDG*

Received: *June 29, 2015* ***Accepted:*** *August 28, 2015* ***Published:*** *September 10, 2015*

ABSTRACT

Background: The *APOE* effect on Alzheimer Disease (AD) risk is stronger in women than in men but its mechanisms have not been established. We assessed the *APOE*-by-sex interaction on core CSF biomarkers, brain metabolism and structure in healthy elderly control individuals (HC).

Methods: Cross-sectional study. HC from the Alzheimer's Disease Neuroimaging Initiative with available CSF (*n* = 274) and/or 3T-MRI (*n* = 168) and/or a FDG-PET analyses (*n* = 328) were selected. CSF amyloid-ß$_{1-42}$ (Aß$_{1-42}$), total-tau (t-tau) and phospho-tau (p-tau$_{181p}$) levels were measured by Luminex assays. We analyzed the *APOE*-by-sex interaction on the CSF biomarkers in an analysis of covariance (ANCOVA). FDG uptake was analyzed by SPM8 and cortical thickness (CTh) was measured by FreeSurfer. FDG and CTh difference maps were derived from interaction and group analyses.

Results: *APOE4* carriers had lower CSF Aß$_{1-42}$ and higher CSF p-tau$_{181p}$ values than non-carriers, but there was no *APOE*-by-sex interaction on CSF biomarkers. The *APOE*-by-sex interaction on brain metabolism and brain structure was significant. Sex stratification showed that female *APOE4* carriers presented widespread brain hypometabolism and cortical thinning compared to female non-carriers whereas male

***APOE4* carriers showed only a small cluster of hypometabolism and regions of cortical thickening compared to male non-carriers.**

Conclusions: The impact of *APOE4* on brain metabolism and structure is modified by sex. Female *APOE4* carriers show greater hypometabolism and atrophy than male carriers. This *APOE*-by-sex interaction should be considered in clinical trials in preclinical AD where *APOE4* status is a selection criterion.

INTRODUCTION

The apolipoprotein E (*APOE*) genotype is the strongest genetic risk factor for Alzheimer's disease (AD) [1]. It has three isoforms, ε2, ε3 and ε4. The *APOE* ε4 allele (*APOE4*) increases the risk for AD [2]. The effect of the *APOE4* allele on AD biomarkers in healthy controls (HC) has been widely studied [3], [4]. *APOE4* carriers have consistently lower cerebrospinal fluid (CSF) ß-amyloid 1–42 ($Aß_{1–42}$) levels than non-carriers, but the differences in tau levels are more controversial [5]–[7]. Most, [8]–[10] but not all [18F]-fluorodeoxyglucose (FDG) PET studies [11]–[13] have shown hypometabolism in AD-related regions in *APOE4* carriers in late-middle age [8] and even earlier [10]. A gene-dosage effect on the hypometabolism has also been reported [9]. The relationship between the *APOE* genotype and brain structure is more controversial. Many cross-sectional studies have reported cortical thinning or hippocampal atrophy, [3], [4], [14] while several others have found no relationship [15] and two have reported increased gray matter in relation to the *APOE4* allele [16], [17].

Several factors might account for the conflicting results. First, the age-range differences between studies are critical because distinct effects of *APOE* across the lifespan have been described [18]. Not all brain changes associated with the *APOE* genotype reflect incipient AD. *APOE* has been implicated in normal human brain development [19]. Second, there are amyloid dependent [20] and independent [21] mechanisms underlying the *APOE* influences on AD risk. However, most studies assessing the role of *APOE* on brain structure and metabolism do not assess AD pathophysiological biomarkers to disentangle these mechanisms. Third, *APOE4* is likely to interact with other pathological factors, complicating the isolation of a unique genetic effect [4]. And fourth, some of the inconsistent imaging and biochemical findings related to *APOE* in HC might result from neglecting a possible *APOE*-by-sex interaction [6]. Most studies to date have included sex as a covariate in the analyses but they did not explicitly test for an *APOE*-by-sex interaction.

The finding that the *APOE* effect on AD risk is stronger in women than in men was reported in early studies, [22], [23] confirmed in meta-analyses, [23], [24] and in a recent longitudinal study [6]. However, only two studies have assessed *APOE*-by-sex interactions on AD biomarkers. Altmann et al found a significant interaction for tau in mild cognitive impairment patients [6]. Damoiseaux et al reported a significant *APOE*-by-sex interaction for CSF tau levels and default mode network abnormalities in healthy controls [25].

The interaction between *APOE4* and sex on brain structure and metabolism has not been established. This interaction could affect the design and interpretation of prevention trials in preclinical AD in which APOE is a selection criterion (i.e. the Alzheimer's Prevention Initiative *APOE4* Trial, NIH project number 1UF1AG046150–01). The aim of the present study was to examine the interactions between *APOE4* and sex on brain metabolism and structure, based on the hypothesis that the *APOE4* allele exerts a differential adverse effect on brain metabolism and structure depending on sex.

RESULTS

Demographic and clinical of the participants in the CSF, FDG and MRI subsets are summarized separately in the Table 1. CSF was available in 274 HC individuals, 328 had an FDG PET, 225 had a 3T MRI, and 137 subjects had all three biomarkers. There were no significant differences between the MRI, PET and CSF subsets in age, sex, *APOE* status, MMSE or CSF biomarkers. There were no significant differences in age, *APOE* status, MMSE or CSF biomarkers between males and females in all three subsets. In the FDG and CSF subsets, males had higher years of education than females ($p < 0.001$), but in the MRI subset this difference did not reach significance.

APOE4 carriers had lower CSF $Aß_{1–42}$ values than non-carriers in all three subsets ($p < 0.001$). *APOE4* carriers had higher CSF $p\text{-}tau_{181p}$ values in the three subsets, but these only reached significance in the FDG and CSF subset which had larger sample sizes ($p < 0.001$ and $p = 0.004$ respectively). *APOE4* carriers had higher CSF t-tau values in the three subsets, but these only reached significance in the CSF subset ($p < 0.05$). There were no significant differences in MMSE scores or education between *APOE4* carriers compared to non-carriers in any of the subsets. There were no significant differences between males and females in CSF biomarkers. Neither was there an *APOE*-by-sex interaction on CSF $Aß_{1–42,}$ CSF t-tau or CSF $p\text{-}tau_{181p}$ values in the analysis of covariance (ANCOVA) analyses.

Table 1: Demographic, cerebrospinal fluid and clinical data in the CSF, FDG-PET and MRI Alzheimer's Disease Neuroimage Initiative subsets.

		MRI (*N* = 168)	FDG-PET (*N* = 328)	CSF (*N* = 274)
***APOE4* N (%)**		50 (29.76%)	87 (26.5%)	71 (25.9%)
AGE		73.4 (6.02)	74.5 (5.57)	74.4 (5.97)
SEX (% Females)		53.6%	49.4%	50.4%
MMSE		29.1 (1.07)	29.0 (1.24)	29.1 (1.15)
YEARS OF EDUCATION		16.6 (2.55)	16.3 (2.77)	16.3 (2.69)
Aß$_{1–42}$* **	TOTAL	200.7 (49.92)	201.4 (52.46)	200.6 (52.51)
	APOE4−	211.3* (46.32)	213.5* (46.87)	212.1* (47.81)
	APOE4+	175.4* (49.58)	165.2* (51.85)	167.9* (51.87)
p-tau$_{p181}$* **	TOTAL	32.4 (16.41)	30.78 (18.14)	30.48 (17.97)
	APOE4−	31.3 (16.68)	28.3* (15.31)	28.2* (15.23)
	APOE4+	35.0 (15.62)	38.1* (23.38)	36.9*(23.10)
t-tau* **	TOTAL	66.0 (31.88)	68.9 (34.57)	68.4 (32.12)
	APOE4−	65.1 (32.60)	67.0 (34.84)	66.0** (30.29)
	APOE4+	68.2 (30.34)	74.5 (33.41)	75.1** (36.22)

APOE4+ = apolipoprotein E ε4 allele carrier, APOE− = apolipoprotein E ε4 allele non-carrier
Values are expressed as mean (standard deviation) unless specified.
*equals $p < 0.001$ and
**equals $p < 0.05$ for the *APOE4* carriers vs non-carriers comparison within each subset. Note that 137 subjects were included in the three subsets.
***CSF data only available in 146 subjects in the MRI subset and 242 subjects in the PET subset.

APOE-by-sex interaction on brain metabolism

Fig. 1A presents this FDG voxel-wise interaction analysis across the cerebral hemispheres, showing voxels with an *APOE*-by-sex interaction, covaried by age and years of education ($p < 0.005$, $k = 50$). Two clusters emerged, one located mainly in the anterior cingulate region and the other in the temporal region. To analyze the directionality, we isolated the temporal cluster, averaged the FDG uptake, and plotted it in box and whisker plots (Fig. 1B). As shown, this interaction was driven by the decreased metabolism in female *APOE4* carriers and the increased metabolism in male *APOE4* carriers. The main and interactive effects of *APOE4* status and sex on brain metabolism in the ANCOVA analysis were significant in the model (interaction term between *APOE4* status and sex: ß-coefficient = 0.069, standard error [SE] = 0.021, $p = 0.001$; main effect of *APOE4* status: ß-coefficient = –0.037, SE = 0.016, $p = 0.019$; main effect of sex: ß-coefficient = −0.041, SE = 0.018, $p = 0.026$). Similar results were found for the anterior cingulate cluster (not shown).

Fig. 2 shows the sex stratified *APOE4* group analyses for FDG, covaried by age and years of education. Female *APOE4* carriers showed widespread clusters of decreased metabolism ($p < 0.005$) across the whole cerebral cortex in both hemispheres with respect to *APOE4* non-carriers (Fig. 2A). Male *APOE4* carriers showed an isolated cluster of decreased metabolism ($p < 0.005$) in the precuneus with respect to non-carriers (Fig. 2B).

To examine the impact of CSF biomarkers in the *APOE*-by-sex interaction on brain metabolism, we included CSF Aß$_{1–42}$ and CSF p-tau$_{181p}$ as covariates in the analyses. The inclusion of the CSF biomarkers did not significantly alter the results of the *APOE*-by-sex interaction analysis (not shown) nor the female *APOE4* carriers vs non-carriers comparison (Fig. 3A1–3A3). In the male APOE4 carriers vs non-carriers comparison two clusters of increased metabolism emerged in *APOE4* carriers with respect to male non-carriers in prefrontal regions and a cluster in the medial temporal region when CSF Aß$_{1–42}$ levels or both Aß$_{1–42}$ and CSF p-tau$_{181p}$ levels (but not CSF p-tau$_{181p}$ levels alone, Fig. 3 B2) were included as a covariate (Fig. 3B1 and 3B3).

APOE-by-sex interaction on brain structure

Fig. 4A presents the vertex-wise interaction analysis across the whole cortical mantle, covaried by age and years of education, showing voxels with

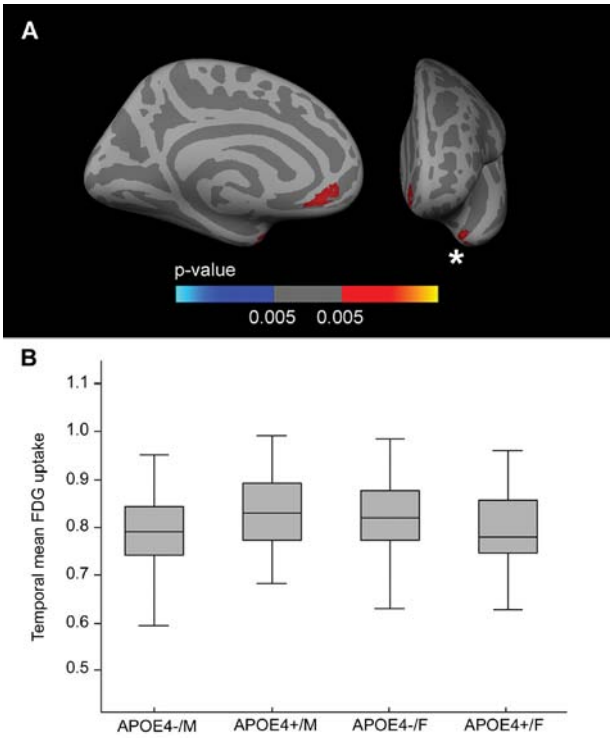

Figure 1: FDG *APOE*-by-sex interaction analysis. A. Areas in which there is a FDG-uptake interaction between sex and the *APOE4* status ($p < 0.005$ uncorrected) co-varied for age and years of education displayed across the medial and frontal views of the cerebral cortex. **B.** Box and whisker plot illustrating individual FDG-uptake values in the temporal cluster. For each plot, the central black lines show the median value, the regions above and below the black line show the upper and lower quartiles, respectively, and the whiskers extend to the minimum and maximum values. As illustrated, the female *APOE4* carriers showed decreased metabolism in the temporal cortex with respect to female non-carriers. FDG = fluorodeoxyglucose; *APOE* = apolipoprotein E, *APOE4*+ = apolipoprotein E ε4 allele carriers, *APOE4*− = apolipoprotein E ε4 allele non-carriers.

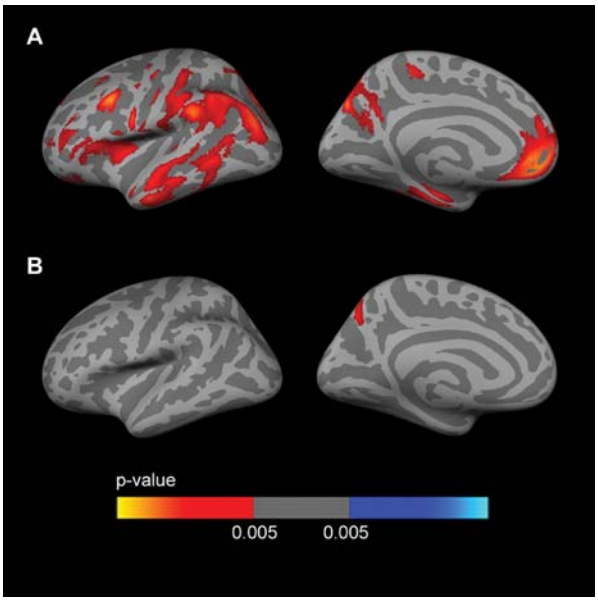

Figure 2: Sex-stratified FDG analyses. Analysis between *APOE4* carriers and *APOE4* non-carriers ($p < 0.005$ uncorrected) in **A.** females and **B.** males, co-varied for age and years of education across the lateral and medial views of the cerebral cortex. As shown, female *APOE4* carriers showed widespread clusters of decreased metabolism with respect to female *APOE4* non-carriers (Fig. 2A), whereas male *APOE4* carriers only showed an isolated cluster of decreased metabolism ($p < 0.005$) in the precuneus with respect to male non-carriers (Fig. 2B). FDG = fluorodeoxyglucose; *APOE4* = apolipoprotein E ε4 allele.

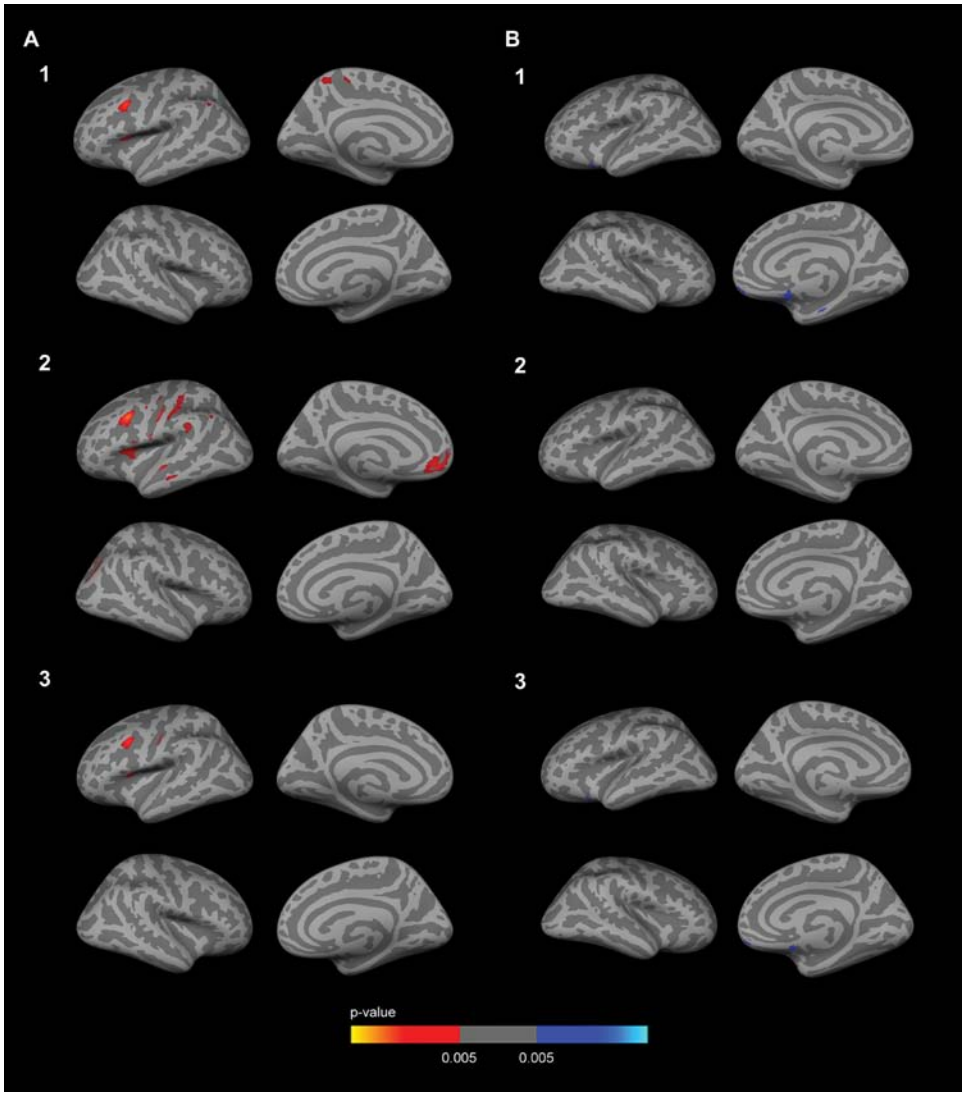

Figure 3: Sex-stratified FDG analyses with CSF biomarker levels included as a covariate. Row 1. CSF $A\beta_{1-42}$ levels; Row 2. CSF p-tau_{181p} levels; Row 3 CSF $A\beta_{1-42}$ and p-tau_{181p} levels. The analysis between female *APOE4* carriers and female *APOE4* non-carriers **A1-A3.** showed several clusters of decreased metabolism ($p < 0.005$ uncorrected) co-varied for age. As illustrated, female *APOE4* carriers showed decreased metabolism in the anterior cingulate cortex with respect to female non-carriers after the inclusion of the CSF biomarkers as a covariate. The analysis between male *APOE4* carriers and male *APOE4* non-carriers **B1-B3.** showed several clusters of increased metabolism ($p < 0.005$ uncorrected) co-varied for age. As illustrated, male *APOE4* carriers showed increased metabolism in several clusters in the dorsolateral prefrontal cortex with respect to male *APOE4* non-carriers after the inclusion of CSF $A\beta_{1-42}$ levels or both CSF $A\beta_{1-42}$ and CSF p-tau_{181p} as a covariate (B1 and B3), but not after the inclusion of the CSF p-tau_{181p} levels alone (B2). FDG = fluorodeoxyglucose; *APOE* = apolipoprotein E, *APOE4*: apolipoprotein E ε4 allele

an *APOE*-by-sex interaction. Two large clusters (Family-wise error corrected [FWE] $p < 0.05$) emerged, one in the dorsolateral frontal region and one in the temporoparietal region. To analyze the directionality, we then isolated the temporoparietal cluster, averaged the cortical thickness (CTh), and plotted it in a box and whisker plot (Fig. 4B). As shown, this interaction was mainly driven by the increased CTh in male *APOE4* carriers. The main effects and the interactive effects of *APOE4* status and sex in the ANCOVA analysis were significant in the model (interaction term between *APOE4* status and sex: ß-coefficient = −0.228, SE = 0.045, $p < 0.001$; main effect of sex: ß-coefficient = 0.149, SE = 0.039, $p < 0.001$; main effect of *APOE4* status: ß-coefficient = 0.062, SE = 0.030, $p = 0.041$). Similar results were found for the remaining cluster (not shown).

Fig. 5 shows the sex-stratified *APOE4* CTh analyses, covaried by age and years of education. Male *APOE4* carriers showed 3 large clusters (FWE corrected) of increased CTh with respect to non-carriers. Two of the clusters were observed in the left hemisphere, one in the dorsolateral frontal region and another in the

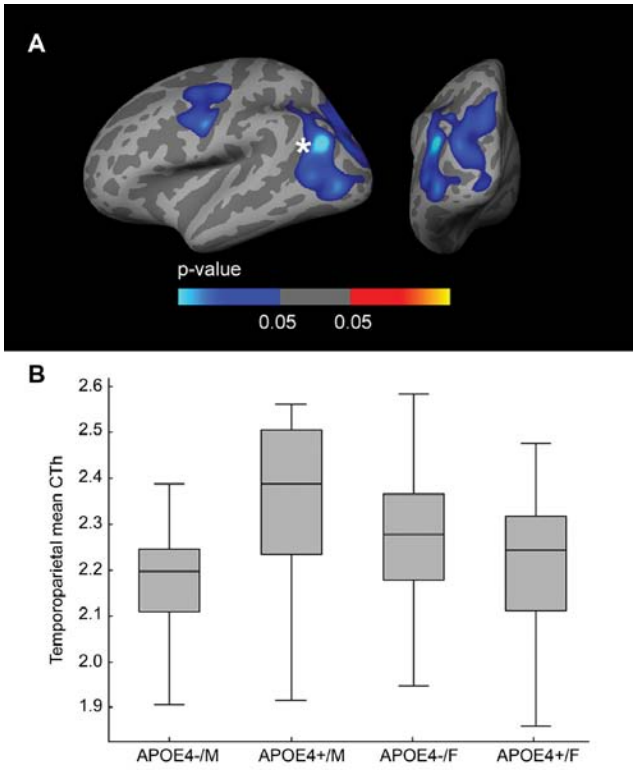

Figure 4: CTh *APOE*-by-Sex interaction analysis. A. Family-wise corrected ($p < 0.05$) clusters with an interaction between sex and the dichotomized *APOE4* genotype co-varied for age and years of education displayed across the lateral and posterior views of the cerebral cortex. **B.** Box and whisker plot illustrating individual CTh values in the temporo-parietal and occipital cluster. For each plot, the central black lines show the median value, regions above and below the black line show the upper and lower quartiles, respectively, and the whiskers extend to the minimum and maximum values. As illustrated, male *APOE4* carriers showed increased CTh in the temporo-parietal and occipital cluster. CTh = cortical thickness; *APOE* = apolipoprotein E, *APOE4*+ = apolipoprotein E ε4 allele carriers, *APOE4*− = apolipoprotein E ε4 allele non-carriers.

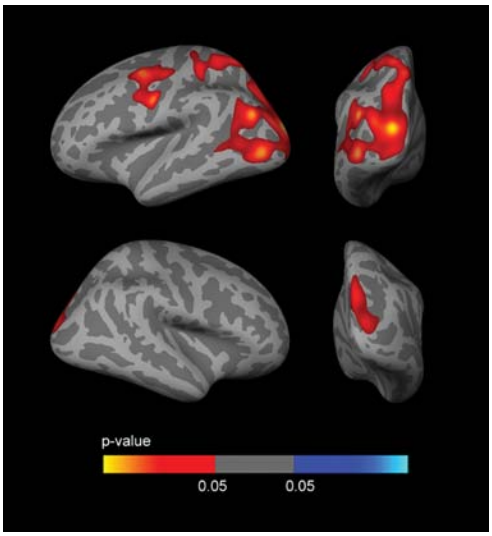

Figure 5: Sex-stratified CTh analyses. Analysis between male *APOE4* carriers and male *APOE4* non-carriers, co-varied for age and years of education. As shown, male *APOE4* carriers presented large clusters of increased CTh (FWE $p < 0.05$) in temporo-parieto-occipital regions, mainly in the left hemisphere. The analysis between female *APOE4* carriers and female *APOE4* non-carriers showed clusters of decreased CTh which did not survive FWE correction (not shown). CTh = cortical thickness; *APOE* = apolipoprotein E; FWE = family-wise error corrected ($p < 0.05$).

temporoparietal, occipital and precuneus regions. The third cluster was observed in the right hemisphere in the parietal and occipital regions. Female *APOE4* carriers showed cortical thinning in several regions than female *APOE4* non-carriers (not shown as this analysis did not survive FWE correction).

To examine the influence of CSF biomarkers on the *APOE*-by-sex interaction on brain structure, we included CSF $A\beta_{1-42}$ and CSF p-tau_{181p} as covariates in the analyses. The vertex-wise *APOE*-by-sex interaction analysis across the whole cortical mantle showed a reduction in the significance maps when including CSF biomarkers as covariates, especially $A\beta_{1-42}$ (Fig. 6). In the sex-stratified *APOE4* CTh analyses, the clusters of increased CTh in male *APOE4* carriers disappeared when CSF $A\beta_{1-42}$ levels (but not CSF p-tau_{181p} levels) were included as a covariate (Fig. 7). No result survived FWE correction in females.

All analyses were repeated excluding APOE ε2 allele carriers and including CSF t-tau as a covariate. We also restricted the analyses to non-hispanic white subjects (not shown). The results were not significantly altered in any case.

DISCUSSION

This study shows for the first time that the impact of the *APOE4* genotype on brain structure and metabolism is modified by sex. We found a significant *APOE*-by-sex interaction on brain metabolism and structure. Female *APOE4* carriers showed brain hypometabolism and cortical thinning with respect to female non-carriers whereas male *APOE4* carriers showed only a small cluster of hypometabolism and cortical thickening with respect to male non-carriers. CSF core AD biomarkers had an influence on brain structural results (and to a lesser extent on brain metabolism).

Epidemiologically, there is strong evidence that supports the *APOE*-by-sex interaction [6], [11], [23]. The only study assessing the *APOE*-by-sex interactions on MRI demonstrated the interaction on resting state functional connectivity but not on gray matter volume [25]. Our results expand these findings. We show an *APOE*-by-sex interaction on both brain structure and metabolism. The discrepancy on brain structure could be due to the differences in the subject population or technical differences (CTh analyses vs voxel-based morphometry [26]). Our FDG results are congruent with those of the aforementioned resting state functional connectivity analyses. *APOE* appears to affect brain network activity which is closely related to neuroenergetic functions [27].

Our metabolic findings suggest that women are metabolically more susceptible to the *APOE4* genotype. Neglecting a possible *APOE*-by-sex interaction on brain metabolism could be one of the reasons for the discordant FDG results [8]–[13]. Male *APOE4* carriers showed increased CTh and females decreased CTh. The finding of cortical thickening in AD vulnerable areas in middle aged (48–75 years old) *APOE4* carriers with respect to non-carriers has already been described [16], [17], but it is in contrast with other works assessing older cohorts [3], [4], [14], [15].

The discrepancies on brain structure might be conciliated if we consider a 2-phase phenomenon model in preclinical AD [28]. In this framework, pathological cortical thickening associated with low CSF $A\beta_{1-42}$ would be followed by atrophy once CSF p-tau_{181p} becomes abnormal [28]. Accordingly, our study shows that the clusters of increased CTh in male *APOE4* carriers disappear when we included CSF $A\beta_{1-42}$ as a covariate. The hypometabolism in female *APOE4* carriers did not disappear when CSF $A\beta_{1-42}$ levels were included as a covariate. The *APOE4* genotype might therefore exert its effects on brain glucose metabolism—at least in part—independently of amyloidogenic pathways [29]. Of note, the inclusion of CSF $A\beta_{1-42}$ levels as a covariate prompted the emergence of several areas of increased metabolism in male *APOE4* carriers. Increased brain metabolism in relation to brain amyloidosis has been previously described [30].

Altogether, our findings support that the mechanisms underlying the increased AD risk in female *APOE4* carriers might occur downstream of Aß pathology [6]. The *APOE4* effect on lowering CSF $A\beta_{1-42}$ levels is marked in both men and women (with no sex differences) and was also found in our work [6], [25]. The impact of an *APOE*-by-sex interaction on CSF has only been assessed twice and, as in the present work, always with data from the ADNI study. The absence of an *APOE*-by-sex interaction on CSF $A\beta_{1-42}$ levels is in agreement with the two previous works [6], [25]. The impact on CSF p-tau_{181p} levels is less clear. We did not find an *APOE*-by-sex interaction on CSF p-tau_{181p} levels. Such an interaction was reported initially [25] in HC but was not confirmed in the later work with a larger sample size [6]. Nonetheless, this last work did find the interaction for CSF p-tau_{181p} levels in mild cognitive impairment patients. Women, moreover, would be more susceptible and would present more abnormal neuronal injury biomarkers [25] and faster clinical decline [6]. Accordingly, female *APOE4* carriers showed hypometabolism and cortical thinning with respect to non-carriers, suggesting that female *APOE4* carriers might be more advanced in the aforementioned 2-phase phenomenon model in preclinical AD [28].

The mechanisms by which the *APOE* allele modifies the risk for AD have been extensively studied but are not completely understood. Both ß-amyloid-dependent [20] and ß-amyloid-independent [21] mechanisms have been described. *APOE* appears to affect brain network activity and neuroenergetic functions [27] and to increase microglia reactivity at Aβ plaques in mouse

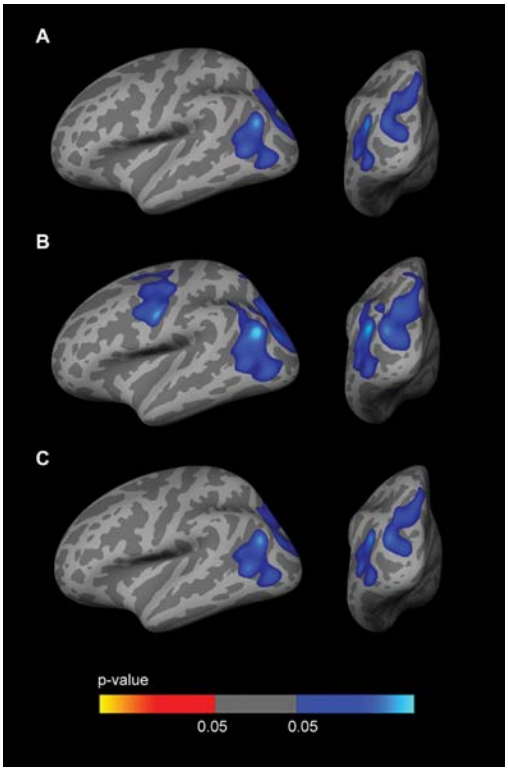

Figure 6: CTh *APOE*-by-Sex interaction analysis with CSF biomarker levels included as covariates. Family-wise corrected ($p < 0.05$) clusters with an interaction between sex and the dichotomized *APOE4* genotype co-varied for age and: **A.** CSF $A\beta_{1-42}$ levels; **B.** CSF p-tau_{181p} levels; **C.** CSF $A\beta_{1-42}$ and p-tau_{181p} levels. As illustrated, the inclusion of CSF $A\beta_{1-42}$ levels as a covariate significantly diminished the clusters showing a CTh *APOE*-by-sex interaction. CTh = cortical thickness; *APOE* = apolipoprotein E.

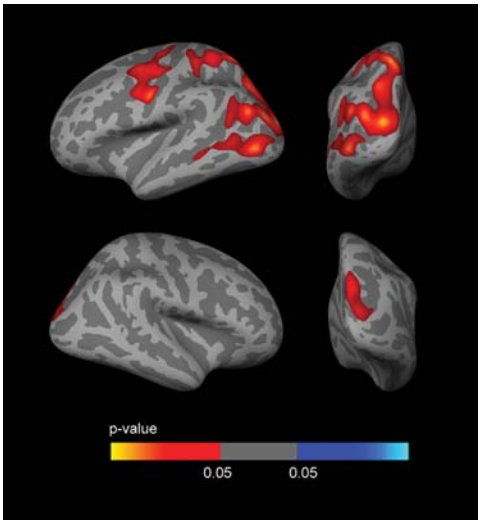

Figure 7: Sex stratified CTh analyses with CSF biomarker levels included as a covariate. The analysis between male *APOE4* carriers and male *APOE4* non-carriers showed several clusters of increased CTh ($p < 0.005$ uncorrected) co-varied for age and CSF p-tau_{181p} levels. There were no significant clusters of increased CTh male *APOE4* carriers vs male *APOE4* non-carriers after the inclusion of CSF $A\beta_{1-42}$ levels as a covariate. CTh = cortical thickness; *APOE* = apolipoprotein E.

models [31], [32]. These metabolic and inflammatory responses in relation to the *APOE* genotype might differ in males and females, accounting for the differences found.

This work has potential clinical implications. Clinical trials in preclinical AD in which *APOE4* status is a selection criterion are underway (Alzheimer's Prevention Initiative *APOE4* Trial, NIH project number 1UF1AG046150–01). Our results emphasize the importance of sex stratification when considering the AD risk and its impact on AD topographical biomarkers [33] conferred by the *APOE* genotype. More broadly, the present work stresses the need to consider interactions between biomarkers and risk factors in the AD preclinical phase [28].

The strengths of this study are the inclusion of a relatively high number of subjects and the fact that the results were found in two different topographical AD biomarkers, [34] with congruent findings between the two. The study has some limitations. It is cross-sectional and the age-range sampled does not include young HC to assess the age-range in which amyloid is starting to deposit in the brain of *APOE4* carriers [35].

In conclusion, the impact of *APOE4* on brain structure and metabolism is modified by sex in HC. This interaction should be considered in current clinical trials in preclinical AD in which *APOE4* status is a selection criterion.

MATERIALS AND METHODS

Study participants and clinical classification

Data used in the preparation of this article were obtained from the Alzheimer's Disease Neuroimaging Initiative (ADNI) database (http://adni.loni.usc.edu). The ADNI was launched in 2003 by the National Institute on Aging (NIA), the National Institute of Biomedical Imaging and Bioengineering (NIBIB), the Food and Drug Administration (FDA), private pharmaceutical companies and non-profit organizations, as a $60 million, 5-year public-private partnership. The primary goal of ADNI has been to test whether serial magnetic resonance imaging (MRI), positron emission tomography (PET), other biological markers, and clinical and neuropsychological assessment can be combined to measure the progression of mild cognitive impairment (MCI) and early AD. Determination of sensitive and specific markers of very early AD progression is intended to aid researchers and clinicians to develop new treatments and monitor their effectiveness, as well as lessen the time and cost of clinical trials.

The Principal Investigator of this initiative is Michael W. Weiner, MD, VA Medical Center and University of California – San Francisco. ADNI is the result of efforts of many co-investigators from a broad range of academic institutions and private corporations, and subjects have been recruited from over 50 sites across the U.S. and Canada. The initial goal of ADNI was to recruit 800 subjects but ADNI has been followed by ADNI-GO and ADNI-2. To date these three protocols have recruited over 1500 adults, ages 55 to 90, to participate in the research, consisting of cognitively normal older individuals (HC), people with early or late MCI, and people with early AD. The follow up duration of each group is specified in the protocols for ADNI-1, ADNI-2 and ADNI-GO. Subjects originally recruited for ADNI-1 and ADNI-GO had the option to be followed in ADNI-2. For up-to-date information, see http://www.adni-info.org.

We included all HC with available CSF and/or a 3T-MRI and/or an FDG PET.

CSF analyses

ADNI procedure

Methods for CSF acquisition and biomarker measurement using the ADNI cohort have been reported previously [36]. $A\beta_{1-42}$, total tau (t-tau) and phospho-tau ($p\text{-}tau_{181p}$) levels were measured using the multiplex xMAP Luminex platform (Luminex) with Innogenetics (INNO-BIA AlzBio3) immunoassay kit–based reagents.

MRI and FDG-PET imaging procedures

ADNI acquisition procedure

The details of MRI and FDG-PET acquisition are available elsewhere (http://www.adni-info.org).

FDG-PET processing procedure

FDG-PET images were downloaded in the most processed format. They were intensity-scaled by the reference pons-vermis region [37], spatially normalized using SPM8 [http://www.fil.ion.ucl.ac.uk/spm/] to the Montreal Neurological Institute (MNI) PET template and spatially smoothed with a Gaussian kernel of full width at half-maximum (FWHM) of 8 mm. All resulting images were visually inspected to check for possible registration errors. Voxel-wise results were displayed at $p < 0.005$ (uncorrected) using an extent threshold $k = 50$, and projected on an inflated single-subject cortical surface reconstruction.

Cortical thickness processing procedure

Cortical reconstruction of the structural images was performed with the FreeSurfer software package, version 5.1 (http://surfer.nmr.mgh.harvard.edu). The procedures have been fully described elsewhere [38]. Estimated surfaces were inspected to detect errors in the automatic segmentation procedure. Fifty-seven of the 225 N3 processed MRI analyzed were excluded because

of segmentation errors and 168 were included in the analyses. A Gaussian kernel of 15 mm full-width at half maximum was applied. To avoid false positives, we tested Monte Carlo simulation with 10,000 repeats in Qdec (family-wise error [FWE], $p < 0.05$). Only regions that survived FWE are presented in the figures.

Statistical methods

Group analyses were made using SPSS (SPSS Inc, Chicago, IL). Comparisons between groups were performed using the two-tailed Student *t* test for continuous variables and a chi-square test for categorical variables.

The main objective of our work was to study the *APOE*-by-sex interaction on brain metabolism and brain structure. Two approaches were used: interaction and sex-stratified analyses. We carried out an ANCOVA as implemented in SPM and FreeSurfer for the PET and MRI analyses, respectively, using the *APOE* genotype (*APOE4* carrier vs *APOE4* non-carrier) and sex as binary categorical independent variables, and age and years of education as variables of no interest to assess the interaction.

To examine the impact of CSF biomarkers on the FDG PET and CTh analyses, we introduced CSF biomarkers as covariates in the analyses. All analyses were repeated excluding *APOE2* carriers and restricting to only non-hispanic white subjects.

Clusters derived from the interaction analyses in FDG or CTh were isolated to analyze the directionality of the interactive effects for each variable within an ANCOVA model, using age as a covariate. Specifically, we used the following model for FDG-PET and MRI:

Mean cluster FDG uptake (or mean cluster CTh) = $\hat{a}_0 + \hat{a}_1$*SEX + $\hat{a}_2$**APOE* + $\hat{a}_3$*[SEX**APOE*] + age

The same ANCOVA approach was used for the CSF analyses to test for an interactive effect of *APOE* genotype and sex in CSF biomarker levels.

ACKNOWLEDGMENTS

We thank Carolyn Newey for editorial assistance.

FUNDING

This work was supported by research grants from the Carlos III Institute of Health, Spain (grants PI11/02425 and PI14/01126 to Juan Fortea, grants PI10/1878 and PI13/01532 to Rafael Blesa and PI11/03035 to Alberto Lleó) and the CIBERNED program (Program 1, Alzheimer Disease to Alberto Lleó), partly funded by FEDER funds of the EU. This work has also been supported by a "Marató TV3" grant (531/U/2014 to Juan Fortea). The work of Frederic Sampedro is supported by the Spanish government FPU (Formación del Profesorado Universitario) doctoral grant (Grant No. AP2012–0400). This work was also supported by NIH-NIA grants to M.J. de Leon, AG022374, AG13616, and AG12101.

Data collection and sharing for this project was funded by the Alzheimer's Disease Neuroimaging Initiative (ADNI) (National Institutes of Health Grant U01 AG024904) and DOD ADNI (Department of Defense award number W81XWH-12–2-0012). ADNI is funded by the National Institute on Aging, the National Institute of Biomedical Imaging and Bioengineering, and through generous contributions from the following: Alzheimer's Association; Alzheimer's Drug Discovery Foundation; BioClinica, Inc.; Biogen Idec Inc.; Bristol-Myers Squibb Company; Eisai Inc.; Elan Pharmaceuticals, Inc.; Eli Lilly and Company; F. Hoffmann-La Roche Ltd and its affiliated company Genentech, Inc.; GE Healthcare; Innogenetics, N.V.; IXICO Ltd.; Janssen Alzheimer Immunotherapy Research & Development, LLC.; Johnson & Johnson Pharmaceutical Research & Development LLC.; Medpace, Inc.; Merck & Co., Inc.; Meso Scale Diagnostics, LLC.; NeuroRx Research; Novartis Pharmaceuticals Corporation; Pfizer Inc.; Piramal Imaging; Servier; Synarc Inc.; andTakeda Pharmaceutical Company. The Canadian Institutes of Health Research is providing funds tosupport ADNI clinical sites in Canada. Private sector contributions are facilitated by the Foundation for the National Institutes of Health (http://www.fnih.org). The grantee organization is the Northern California Institute for Research and Education, and the study is coordinated by the Alzheimer's Disease Cooperative Study at the University of California, San Diego. ADNI data are disseminated by the Laboratory for Neuro Imaging at the University of Southern California.

CONFLICTS OF INTEREST

All authors report no biomedical financial interests or potential conflicts of interest related to this work.

REFERENCES

1. Corder EH, Saunders AM, Strittmatter WJ, Schmechel DE, Gaskell PC, Small GW, Roses AD, Haines JL, Pericak-Vance MA. Gene dose of apolipoprotein E type 4 allele and the risk of Alzheimer,'s disease in late onset families. Science. 1993; Aug 261:921–3.
2. Liu C-C, Liu C-C, Kanekiyo T, Xu H, Bu G. Apolipoprotein E and Alzheimer disease: risk, mechanisms and therapy. Nat. Rev. Neurol. 2013; Feb 9:106–18.
3. Liu Y, Yu J-T, Wang H-F, Han P-R, Tan C-C, Wang C, Meng X-F, Risacher SL, Saykin AJ, Tan L. APOE genotype and neuroimaging markers of Alzheimer's disease: systematic review and meta-analysis. J. Neurol. Neurosurg. Psychiatry. 2015; May 86:127–34.

4. Reinvang I, Espeseth T, Westlye LT. APOE-related biomarker profiles in non-pathological aging and early phases of Alzheimer's disease. Neurosci. Biobehav. Rev. 2013; May 37:1322–1335.
5. Sunderland T, Mirza N, Putnam KT, Linker G, Bhupali D, Durham R, Soares H, Kimmel L, Friedman D, Bergeson J, Csako G, Levy JA, Bartko JJ, Cohen RM. Cerebrospinal fluid beta-amyloid1-42 and tau in control subjects at risk for Alzheimer's disease: the effect of APOE epsilon4 allele. BiolPsychiatry. 2004; Nov 56:670–6.
6. Altmann A, Tian L, Henderson VW, Greicius MD. Sex modifies the APOE-related risk of developing Alzheimer disease. AnnNeurol. 2014; Apr 75:563–73.
7. Vemuri P, Wiste HJ, Weigand SD, Knopman DS, Shaw LM, Trojanowski JQ, Aisen PS, Weiner M, Petersen RC, Jack CR. Effect of apolipoprotein E on biomarkers of amyloid load and neuronal pathology in Alzheimer disease. AnnNeurol. 2010; Mar 67:308–16.
8. Reiman EM, Caselli RJ, Yun LS, Chen K, Bandy D, Minoshima S, Thibodeau SN, Osborne . Preclinical evidence of Alzheimer's disease in persons homozygous for the epsilon 4 allele for apolipoprotein E. N. Engl. J. Med. 1996; Mar 334:752–8.
9. Reiman EM, Chen K, Alexander GE, Caselli RJ, Bandy D, Osborne D, Saunders AM, Hardy J. Correlations between apolipoprotein E epsilon4 gene dose and brain-imaging measurements of regional hypometabolism. Proc. Natl. Acad. Sci. U. S. A. 2005; Jun 102:8299–302.
10. Reiman EM, Chen K, Alexander GE, Caselli RJ, Bandy D, Osborne D, Saunders AM, Hardy J. Functional brain abnormalities in young adults at genetic risk for late-onset Alzheimer's dementia. Proc. Natl. Acad. Sci. U. S. A. 2004; Jan 101:284–9.
11. Corder EH, Jelic V, Basun H, Lannfelt L, Valind S, Winblad B, Nordberg A. No difference in cerebral glucose metabolism in patients with Alzheimer disease and differing apolipoprotein E genotypes. ArchNeurol. 1997; Mar 54:273–7.
12. Hirono N, Mori E, Yasuda M, Imamura T, Shimomura T, Hashimoto M, Tanimukai S, Kazui H, Yamashita H. Lack of effect of apolipoprotein E E4 allele on neuropsychiatric manifestations in Alzheimer's disease. J. Neuropsychiatry Clin. Neurosci. 1999; Jan 11:66–70.
13. Samuraki M, Matsunari I, Chen W-P, Shima K, Yanase D, Takeda N, Matsuda H, Yamada M. Glucose metabolism and gray-matter concentration in apolipoprotein E ε4 positive normal subjects. NeurobiolAging. 2012; Oct 33:2321–3.
14. Cherbuin N, Leach LS, Christensen H, Anstey KJ. Neuroimaging and APOE genotype: a systematic qualitative review. Dement. Geriatr. Cogn. Disord. 2007; Jan 24:348–62.
15. Novak NM, Stein JL, Medland SE, Hibar DP, Thompson PM, Toga AW. EnigmaVis: online interactive visualization of genome-wide association studies of the Enhancing NeuroImaging Genetics through Meta-Analysis (ENIGMA) consortium. Twin Res. Hum. Genet. 2012; Jun 15:414–8.
16. Espeseth T, Westlye LT, Fjell AM, Walhovd KB, Rootwelt H, Reinvang I. Accelerated age-related cortical thinning in healthy carriers of apolipoprotein E epsilon 4. NeurobiolAging. 2008; Mar 29:329–340.
17. Espeseth T, Westlye LTL, Walhovd KKB, Fjell AM, Endestad T, Rootwelt H, Reinvang I. Apolipoprotein E ε4-related thickening of the cerebral cortex modulates selective attention. NeurobiolAging. 2012; Mar 33:304–322.e1.
18. Filippini N, Ebmeier KP, MacIntosh BJ, Trachtenberg AJ, Frisoni GB, Wilcock GK, Beckmann CF, Smith SM, Matthews PM, Mackay CE. Differential effects of the APOE genotype on brain function across the lifespan. Neuroimage. 2011; Jan 54:602–10.
19. Dean DC, Jerskey BA, Chen K, Protas H, Thiyyagura P, Roontiva A, O'Muircheartaigh J, Dirks H, Waskiewicz N, Lehman K, Siniard AL, Turk MN, Hua X, Madsen SK, Thompson PM, Fleisher AS, Huentelman MJ, Deoni SCL, Reiman EM. Brain differences in infants at differential genetic risk for late-onset Alzheimer disease: a cross-sectional imaging study. JAMA Neurol. 2014; Jan 71:11–22.
20. Holtzman DM, Herz J, Bu G. Apolipoprotein E and apolipoprotein E receptors: normal biology and roles in Alzheimer disease. Cold Spring Harb. Perspect. Med. 2012; Mar 2:a006312.
21. Wolf AB, Valla J, Bu G, Kim J, LaDu MJ, Reiman EM, Caselli RJ. Apolipoprotein E as a β-amyloid-independent factor in Alzheimer's disease. Alzheimers. Res. Ther. 2013; Jan 5:38.
22. Poirier J, Davignon J, Bouthillier D, Kogan S, Bertrand P, Gauthier S. Apolipoprotein E polymorphism and Alzheimer's disease. Lancet. 1993; Sep 342:697–9.
23. Payami H, Montee KR, Kaye JA, Bird TD, Yu CE, Wijsman EM, Schellenberg GD. Alzheimer's disease, apolipoprotein E4, and gender. JAMA. 1994; May 271:1316–7.
24. Farrer LA, Cupples LA, Haines JL, Hyman B, Kukull WA, Mayeux R, Myers RH, Pericak-Vance MA, Risch N, van Duijn CM. Effects of age, sex, and ethnicity on the association between apolipoprotein E genotype and Alzheimer disease. A meta-analysis. APOE and Alzheimer Disease Meta Analysis Consortium. JAMA. 278:1349–561997.
25. Damoiseaux JS, Seeley WW, Zhou J, Shirer WR, Coppola G, Karydas A, Rosen HJ, Miller BL, Kramer JH, Greicius MD. Gender modulates the APOE ε4 effect in healthy older adults: convergent evidence from functional brain connectivity and spinal fluid tau levels. JNeurosci. 2012; Jun 32:8254–62.
26. Fortea J, Sala-Llonch R, Bartrés-Faz D, Bosch B, Lladó A, Bargalló N, Molinuevo JL, Sánchez-Valle R. Increased cortical thickness and caudate volume precede atrophy in PSEN1 mutation carriers. J. Alzheimers. Dis. 2010; Jan 22:909–22.

27. Wolf AB, Caselli RJ, Reiman EM, Valla J. APOE and neuroenergetics: an emerging paradigm in Alzheimer's disease. NeurobiolAging. 2013; Apr 34:1007–17.

28. Fortea J, Vilaplana E, Alcolea D, Carmona-Iragui M, Sánchez-Saudinos M-B, Sala I, Antón-Aguirre S, González S, Medrano S, Pegueroles J, Morenas E, Clarimón J, Blesa R, Lleó A. Cerebrospinal Fluid ß-Amyloid and Phospho-Tau Biomarker Interactions Affecting Brain Structure in Preclinical Alzheimer Disease. AnnNeurol. 2014; May :1–8.

29. Jagust WJ, Landau SM. Apolipoprotein E, not fibrillar β-amyloid, reduces cerebral glucose metabolism in normal aging. JNeurosci. 2012; Dec 32:18227–33.

30. Johnson SC, Christian BT, Okonkwo OC, Oh JM, Harding S, Xu G, Hillmer AT, Wooten DW, Murali D, Barnhart TE, Hall LT, Racine AM, Klunk WE, a Mathis C, Bendlin BB, Gallagher CL, Carlsson CM, a Rowley H, Hermann BP, Dowling NM, Asthana S, a Sager M. Amyloid burden and neural function in people at risk for Alzheimer's Disease. NeurobiolAging. 2014; Mar 35:576–84.

31. Rodriguez GA, Tai LM, LaDu MJ, Rebeck GW. Human APOE4 increases microglia reactivity at Aβ plaques in a mouse model of Aβ deposition. JNeuroinflammation. 2014; Jan 11:111.

32. Tai LM, Ghura S, Koster KP, Liakaite V, Maienschein-Cline M, Kanabar P, Collins N, Ben-Aissa M, Lei AZ, Bahroos N, Green S, Hendrickson B, Van Eldik LJ, LaDu MJ. APOE -modulated Aß-induced neuroinflammation in Alzheimer's disease: current landscape, novel data and future perspective. JNeurochem. 2015; Feb.

33. Sperling R, Aisen P, Beckett L. Toward defining the preclinical stages of Alzheimer's disease: Recommendations from the National Institute on Aging-Alzheimer's Association workgroups workgroups on diagnostic guidelines for Alzheimer's disease. 2011; May 7:280–92.

34. Dubois B, Feldman HH, Jacova C, Cummings JL, Dekosky ST, Barberger-Gateau P, Delacourte A, Frisoni G, Fox NC, Galasko D, Gauthier S, Hampel H, Jicha GA, Meguro K, O'Brien J, Pasquier F, Robert P, Rossor M, Salloway S, Sarazin M, de Souza LC, Stern Y, Visser PJ, Scheltens P. Revising the definition of Alzheimer's disease: a new lexicon. Lancet Neurol. 2010; Nov 9:1118–27.

35. Pletnikova O, Rudow G, Hyde T, Kleinman JE, Ali S, Bharadwaj R, Gangadeen S, Crain B, Fowler D, Rubio A, Troncoso J. Alzheimer lesions in the brains of young subjects. Cogn. Behav. Neurol. 2015; In press.

36. Shaw LM, Vanderstichele H, Knapik-Czajka M, Clark CM, Aisen PS, Petersen RC, Blennow K, Soares H, Simon A, Lewczuk P, Dean R, Siemers E, Potter W, Lee V M-Y, Trojanowski JQ, Initiative ADN. Cerebrospinal Fluid Biomarker Signature in Alzheimer's Disease Neuroimaging Initiative Subjects. AnnNeurol. 2009; Apr 65:403–413.

37. Landau S, Jagust W. UC Berkeley FDG MetaROI methods. Alzheimer's Dis. Neuroimaging Initiat. 2011.

38. Fischl B, Dale AM. Measuring the thickness of the human cerebral cortex from magnetic resonance images. Proc. Natl. Acad. Sci. U. S. A. 2000; Sep 97:11050–5.

Molecular Psychiatry (2015) 20, 772–777

www.nature.com/mp

OPEN

ORIGINAL ARTICLE

Telling true from false: cannabis users show increased susceptibility to false memories

J Riba[1,2,3], M Valle[2,3,4,11], F Sampedro[5,11], A Rodríguez-Pujadas[1], S Martínez-Horta[6], J Kulisevsky[6,7] and A Rodríguez-Fornells[8,9,10]

Previous studies on the neurocognitive impact of cannabis use have found working and declarative memory deficits that tend to normalize with abstinence. An unexplored aspect of cognitive function in chronic cannabis users is the ability to distinguish between veridical and illusory memories, a crucial aspect of reality monitoring that relies on adequate memory function and cognitive control. Using functional magnetic resonance imaging, we show that abstinent cannabis users have an increased susceptibility to false memories, failing to identify lure stimuli as events that never occurred. In addition to impaired performance, cannabis users display reduced activation in areas associated with memory processing within the lateral and medial temporal lobe (MTL), and in parietal and frontal brain regions involved in attention and performance monitoring. Furthermore, cannabis consumption was inversely correlated with MTL activity, suggesting that the drug is especially detrimental to the episodic aspects of memory. These findings indicate that cannabis users have an increased susceptibility to memory distortions even when abstinent and drug-free, suggesting a long-lasting compromise of memory and cognitive control mechanisms involved in reality monitoring.

Molecular Psychiatry (2015) **20,** 772–777; doi:10.1038/mp.2015.36; published online 31 March 2015

INTRODUCTION

Cannabis is the most widely used recreational drug worldwide after alcohol and tobacco.[1,2] Despite changing attitudes in the perceived risks associated with this substance and decriminalization initiatives taking place in many US states and countries,[1,3] the health implications of long-term cannabis consumption are still a matter of concern.[4] Regular use of cannabis has been associated with adverse health consequences, including psychiatric and neurocognitive disorders. Besides the more immediate risk of developing cannabis dependence,[5] other mental disorders, such as anxiety, depression or psychosis,[6,7] and cognitive impairment have also been described.[8] One recent study involving over a thousand individuals found that chronic cannabis use is associated with cognitive decline, with greater deterioration being observed in those individuals presenting a more persistent use.[9] Among the various cognitive domains studied, memory is one of the most frequently identified as being negatively affected by cannabis.[9–11]

Impaired working and declarative memory are well-known aspects of acute intoxication.[12] Cannabis preparations and delta-9-tetrahydrocannabinol, its main active principle, acutely deteriorate the ability to retain information for short periods of time,[8,13] and impair episodic memory and verbal recall.[14,15] A characteristic of cannabis consumption is that residual effects can linger for days after the most recent use.[10] Typically, these deleterious effects gradually wear off and memory processes normalize after several weeks of abstinence.[16,17] However, some studies in heavy cannabis users have observed impairment persisting even months after the last consumption.[9,10] In addition to impaired performance, imaging studies in chronic cannabis users have found structural brain alterations in the hippocampus, a key area in the memory processing network. Notably, decreases in hippocampal volume showed an association with the amount of cannabis used.[18–20] These structural changes may be long-lasting, as volume reductions can persist even after abstinence of 6 months.[18]

An unknown aspect of long-term cannabis use is its potential to disrupt memory and reality monitoring mechanisms that normally allow us to distinguish between veridical and illusory events. Avoiding memory distortions may be extremely relevant in certain contexts such as the courtroom and forensic examination, and in a more general context this ability provides us with an adequate sense of reality that guides future behavior based on past experiences. Memories of events that never occurred, or false memories, can be found in neurological and psychiatric conditions. They have been described in post-traumatic stress disorder, psychosis, dissociative disorders and in cases of confabulation or 'honest lying' associated with confessions of uncommitted crimes, among others.[21] However, in a more subtle form, false memories are also a common occurrence in everyday life in healthy individuals[22] and show an increase with age.[23] Susceptibility to this phenomenon probably has a neural basis, as it has been linked to individual differences in white matter microstructure.[24]

[1]Human Neuropsychopharmacology Group, Sant Pau Institute of Biomedical Research (IIB-Sant Pau), Sant Antoni María Claret 167, Barcelona, Spain; [2]Centre d'Investigació de Medicaments, Servei de Farmacologia Clínica, Hospital de la Santa Creu i Sant Pau, Barcelona, Spain; [3]Departament de Farmacologia i Terapèutica, Universitat Autònoma de Barcelona, Centro de Investigación Biomédica en Red de Salud Mental, CIBERSAM, Barcelona, Spain; [4]Pharmacokinetic and Pharmacodynamic Modelling and Simulation, IIB-Sant Pau, Sant Antoni María Claret, Barcelona, Spain; [5]School of Medicine, Universitat Autònoma de Barcelona, Barcelona, Spain; [6]Movement Disorders Unit, Neurology Department, Hospital de la Santa Creu i Sant Pau, Universitat Autònoma de Barcelona. Barcelona, Spain; [7]Centro Investigación Biomedica en Red-Enfermedades Neurodegenerativas (CIBERNED), Spain; [8]Cognition and Brain Plasticity Group (Bellvitge Biomedical Research Institute) IDIBELL, L'Hospitalet de Llobregat, Barcelona, Spain; [9]Department of Basic Psychology, University of Barcelona, Barcelona, Spain and [10]Catalan Institution for Research and Advanced Studies, ICREA, Barcelona, Spain. Correspondence: Dr J Riba, Human Neuropsychopharmacology Group, Sant Pau Institute of Biomedical Research (IIB-Sant Pau), IIB-Sant Pau. C/Sant Antoni María Claret, 167, Barcelona 08025, Spain.
E-mail: jriba@santpau.cat
[11]These authors contributed equally to this work.
Received 29 October 2014; revised 5 February 2015; accepted 13 February 2015; published online 31 March 2015

False memories can be induced in laboratory conditions using experimental procedures such as the Deese-Roediger-McDermott paradigm.[25] In this task, participants study a list of words that are later presented together with semantically unrelated new words and semantically related new words (lures).[25] Lures induce the illusion of a false memory where participants mistakenly claim that the new stimulus has been encountered previously. The correct identification of lures as previously unseen stimuli is more cognitively demanding than that of unrelated novel stimuli, the former leading to greater activation of medial temporal lobe (MTL), parietal and frontal brain regions.[26] In the present study we tested susceptibility to false memories in a group of abstinent heavy cannabis users and their matched controls using the Deese-Roediger-McDermott paradigm in association with functional magnetic resonance imaging (fMRI; see online methods).

MATERIALS AND METHODS

Ethics

The study was approved by the Ethics Committee of Sant Pau Hospital and all participants gave their written consent to participate.

Participants

We recruited a group of 16 heavy cannabis users not seeking or having a history of treatment for their cannabis consumption. We defined heavy cannabis use as daily use for at least the last 2 years. The recruited sample had never been diagnosed with a psychiatric or neurological condition including alcohol or other drug abuse. Cannabis users were matched to a cannabis-naive (<50 occasions of cannabis use in their lifetime) group of healthy controls, free of psychiatric or neurological conditions. Fourteen controls had used cannabis <10 times and only two had used it between 10 and 50 times. To rule out a history of psychiatric and neurological disorders, users and controls were interviewed by a clinical psychologist. The two groups were matched taking into account the following socio-demographic variables: sex, age, years of education, verbal intelligence and fluid intelligence. Verbal intelligence was assessed using a Spanish version of the NART,[27] known as TAP–'Test de Acentuación de Palabras' ('word accentuation test').[28] Fluid intelligence was assessed using a computerized version of the Matrix Reasoning from the Wechsler Adult Intelligence Scale-III.[29] Detailed socio-demographic data for each group is provided as Supplementary information.

Cannabis users had taken the drug an average of around 42 000 times (range: 4 000–246 375) times. The average number of years of use was 21 (3–39). The average number of daily cannabis cigarettes smoked was 5 (1–24) and the average age of initial use was 17 (12–20) years. We did not exclude tobacco smokers from the study and they were not instructed to abstain from tobacco during the study. Ten participants in the cannabis group and four in the control group were currently using tobacco. Participants abstained from cannabis use for at least 4 weeks prior to testing. Urine samples were taken during the 4-week period and immediately before the experimental session. All participants tested negative for cannabis, alcohol, benzodiazepines, amphetamines, opiates and cocaine on their day of participation.

Memory paradigm

The memory paradigm consisted in a modified version of the Deese-Roediger-McDermott paradigm[25] and included a study phase and a testing phase (see Supplementary information). Both phases were conducted with the participant in the MRI scanner. Stimuli were presented using goggles and behavioral responses were recorded by button press using a magnet-compatible response pad.

The study phase comprised 20 lists of four words. Prior to the presentation of the four words comprising a list, the name of that list was announced on the screen. Of the 20 lists, fifteen comprised four semantically related Spanish words and the other 5 lists comprised 3 semantically related words plus a catch word. Catch words were semantically unrelated to the list announced and were used to control for the participant's attention during the task. A total of 80 stimuli were presented during the study phase: 75 legitimate words plus 5 catch words. Participants were requested to indicate by button press whether the presented word belonged to the announced list. The order of presentation of the 20 word lists was randomized between participants. The study phase lasted 11 min.

Approximately 15 min after completion of the study phase, the test phase was conducted and lasted 14 min. Participants were presented with the 75 legitimate words shown during the study phase plus 40 semantically unrelated new words and 40 semantically related new words (lures, see stimuli tables in the Supplementary information file). Stimuli were presented in semi-random order with the restriction that the same type of stimulus (old, new or lure) was not presented more than twice in succession. We used a rapid presentation event-related design. Stimulus duration was 500 ms. The stimulus onset asynchrony was on average 5.125 s and it was jittered between 4 s and 10 s. The order and timing of events were optimized using the Optseq2 software (http://surfer.nmr.mgh.harvard.edu/optseq/). Participants were required to judge whether a word had been presented in the study phase and make an old vs new decision by button press. The task had the following outcomes: (1) a studied word was correctly classified as old or 'hit' (true memory recognition); (2) a studied word was incorrectly classified as new or 'miss'; (3) a non-studied word was correctly classified as new or 'correct rejection of new word'; (4) a non-studied word was incorrectly classified as old or 'false alarm'; (5) a lure was correctly classified as new or 'false memory rejection'; and (6) a lure was incorrectly classified as old or 'false recognition'.

Functional magnetic imaging protocol

Data were acquired in a 3-Tesla Siemens Magnetom Trio Scanner. Structural images of the brain were obtained by means of a T1-weighted MPRAGE sequence: 256×256 matrix; 240 1-mm sagittal slices. Functional images were obtained using an echo-planar-imaging sequence. The pulse-sequence parameters were as follows: time to repeat = 2000 ms; time to echo = 29 ms; flip angle = 80°; matrix = 128×128; slice thickness = 4 mm. Each volume comprised 36 transversal slices ($2\times2\times4$ mm voxel). A total of 412 volumes were acquired during the test phase.

Preprocessing of imaging data

fMRI data were analyzed using the SPM8 software. Raw echo-planar-imaging images were slice time and motion corrected. Echo-planar-imaging images were then co-registered to each individual's structural T1 image. T1 images were normalized to the T1 Montreal Neurologic Institute template and the obtained parameters were used to transform the echo-planar-imaging images into Montreal Neurologic Institute space. Normalized images were subjected to high-pass temporal filtering (128 s or 0.008 Hz) and to spatial smoothing using an 8 mm Gaussian filter.

Statistical analysis

A first-level analysis was performed for each individual using a design matrix that included the following predictors: 'hit', 'miss', 'correct rejection of new word', 'false alarm', 'false memory rejection', 'false recognition'. Motion correction parameters and the temporal and hemodynamic response function dispersion derivatives were introduced in the model as covariates. The contrast of interest 'false memory rejection' > 'correct rejection of new word' was calculated for each participant.

The second level analysis involved a between-groups (cannabis and controls) comparison using an independent-samples *t*-test for the 'false memory rejection' > 'correct rejection of new word' contrast. Both the controls > cannabis and cannabis > controls contrasts were calculated. We considered clusters to be significantly different between groups for *P*-values <0.001 uncorrected and a spatial extension of 10 contiguous voxels.

To assess for correlations between activation values and drug-use variables, mean fMRI parameter values for the different statistically significant clusters (region of interest) were calculated for each individual. The voxels included in the calculations for each cluster were those showing *P*-values <0.001 uncorrected.

RESULTS

Behavior

The analysis of behavioral data obtained in the study phase did not detect differences between groups regarding their degree of attention. Thus, the number of correctly identified catch trials, expressed as mean ± s.d., was 4.00 ± 0.63 for the controls and 4.18 ± 0.75 for the cannabis users $t(30)=-0.76$, $P>0.1$.

The analysis of behavioral data in the test phase showed no differences between groups in the number of correctly recognized studied words (true memory recognition; mean ± s.d.: cannabis users, 64 ± 6; controls, 65 ± 6; $t(30) = 0.4$, $P > 0.1$) or in the number of correctly rejected new words (correct rejection of new words: cannabis users, 37 ± 3; controls, 39 ± 0.7; $t(30) = 1.9$, $P = 0.076$). No differences were found either in the time (in milliseconds) taken to correctly recognize studied words (cannabis users, 1185 ± 199; controls, 1089 ± 195; $t(30) = -1.36$, $P > 0.1$), or to correctly reject new words (cannabis users, 1200 ± 345; controls, 1043 ± 196; $t(30) = -1.58$, $P > 0.1$). However, as shown in Figure 1, cannabis users showed significantly more false memories. A two-way analysis of variance, with outcome (false recognition vs false memory rejection) as within-subjects factor and participant group (cannabis vs controls) as between-subject factors, showed a significant interaction ($F(1,30) = 5.60$, $P = 0.025$). Lure words were falsely recognized as studied words more often (false recognition; cannabis users, 12 ± 6; controls, 8 ± 4; $t(30) = -2.24$, $P = 0.033$), and were rejected less often (false memory rejection; cannabis users, 27 ± 6; controls, 32 ± 4; $t(30) = 2.46$, $P = 0.021$).

fMRI

Imaging data were analyzed specifically looking for differences between groups in the pattern of blood oxygenation level dependent (BOLD) response associated with the correct rejection of lures or false memory rejection as compared with the correct rejection of new words. Figure 2 shows the mentioned contrast separately for each of the two participant groups. Note the larger extension and lower *P*-values of active voxels in the control group.

Figure 3 and Table 1 show the results of the between-groups comparison. Control participants showed higher activation for the contrast false memory rejection > correct rejection of new words in parietal, prefrontal, temporal and subcortical structures. All these structures have previously been found to be involved in the correct identification of false relative to new semantic stimuli.[26] Greater behavioral efficacy in the control group was thus associated with greater brain activity for the rejection of lures than for the rejection of new unrelated words.

Correlation analysis

To look for potential associations between the pattern of brain activation and history of cannabis use, we defined regions of interest for each of the statistically significant areas identified in the between-groups comparison. The parameters (beta values) associated with false memory rejection in each region of interest were extracted only for the cannabis group, and their values were correlated with drug-use data: lifetime cannabis consumption, years of use and amount of cannabis used daily. As shown in Figure 4, a significant negative correlation ($r = -0.806$, $r^2 = 0.650$, $P < 0.001$) was found between activity in the MTL regions of interest and lifetime cannabis use (log value of the estimated number of cannabis cigarettes smoked).

DISCUSSION

Our results show that cannabis users had a higher susceptibility to memory illusions, as observed in certain neurologic and psychiatric populations,[21] and elderly individuals.[23] They further identify the functional substrate of this deficit in the hypoactivation of a series of spatially distributed brain regions participating in the network involved in semantic[30] and episodic[31] retrieval. The network identified fits nicely with previous studies that have shown that compared with new items, recognition of false stimuli leads to greater activation of the hippocampus and the parahippocampal gyrus, and also of the left parietal and left dorsolateral prefrontal cortices in healthy subjects.[26] Although activation of MTL structures in these tasks can be directly

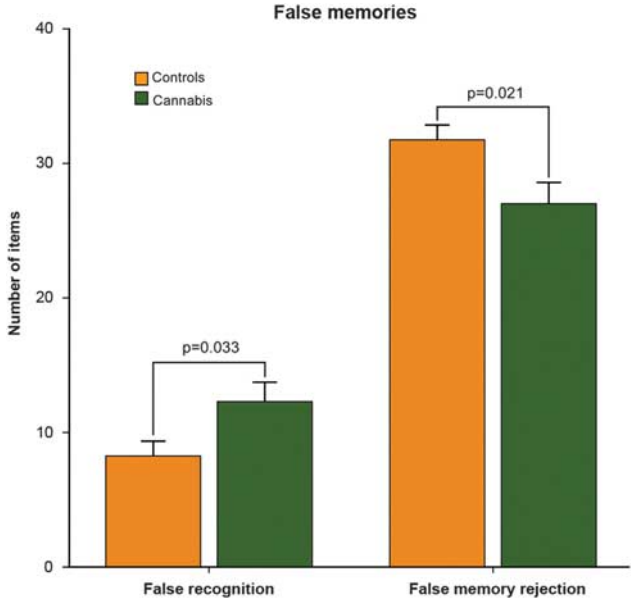

Figure 1. Behavioral data. The graphs show performance results in the memory task. Cannabis users performed significantly worse than controls, showing increased false recognition and decreased false memory rejection. Error bars denote one s.d. of mean.

associated with memory,[32] the parietal cortex can be linked to attentional processes and the dorsolateral prefrontal cortex to monitoring issues in this context.[33] It has been shown that the effective rejection of lures leads to greater activation of the dorsolateral prefrontal cortex[34] and lesions at this level lead to increased false recognition in neurological patients.[35] Thus, rather than a compromise of memory structures per se (that is, the hippocampus), our results point to a more diffuse impairment, which leads to a reduced capacity to deal with the retrieval and monitoring demands needed to differentiate between illusory and real events.

From a theoretical perspective, two main accounts have been put forward to explain the false memory phenomenon: the fuzzy trace theory and the activation-monitoring account. The fuzzy trace theory postulates that stimuli are encoded into two types of memory traces: a 'verbatim' trace containing specific details and features associated with the stimulus, and a 'gist' trace that contains more general aspects of the encoding event. False memories occur when new stimuli share certain features with past events and elicit the retrieval of the gist trace, but not the verbatim trace.[36] In contrast, the activation-monitoring account[37] postulates that cognitive control mechanisms need to be engaged to correctly identify and reject the highly activated lures. According to this view, false memories occur when monitoring mechanisms fail to identify the non-studied but semantically related lures.

Our findings can be interpreted in the light of the two accounts described above. The between-groups comparison of fMRI activation maps showed activity not only in distributed brain areas participating in semantic[30] and episodic[31] retrieval, but also in cognitive control, as suggested by the significant dorsolateral prefrontal clusters identified.[38,39] The greater activation found for the control group in the medial and lateral temporal cortices suggests access to both the semantic (lateral) and episodic (medial) features of the studied stimuli. Using the terminology of the fuzzy trace account, controls would take advantage of both the verbatim and gist traces when deciding to reject a false memory. On the contrary, the inverse correlation found between lifetime cannabis use and the BOLD response in the MTL suggests that chronic exposure to cannabis may be especially detrimental to the brain structure providing the episodic or gist features to

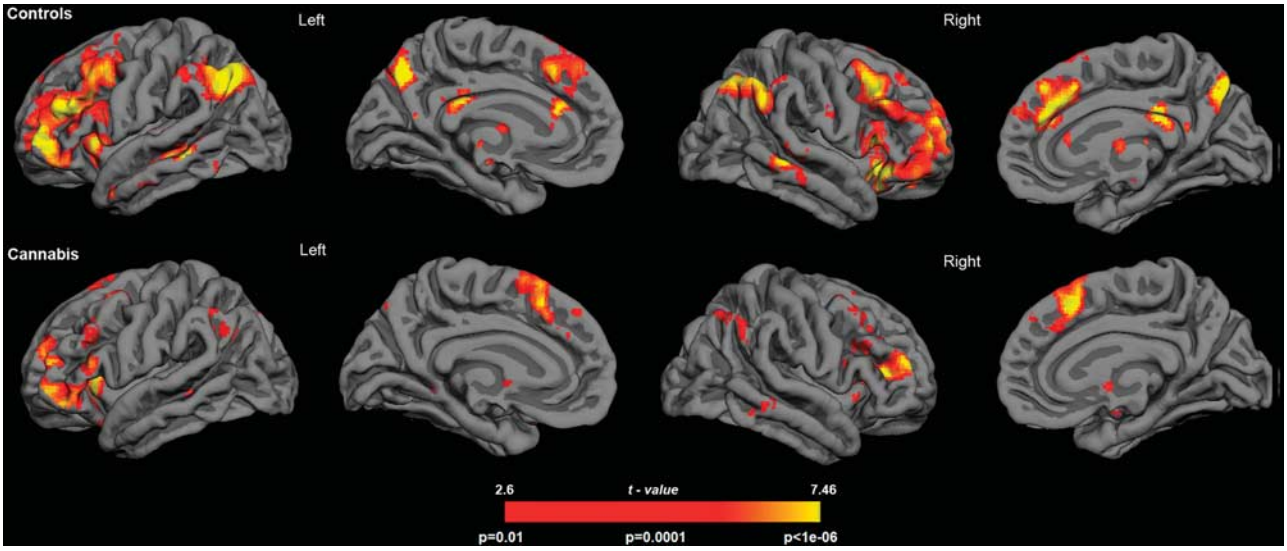

Figure 2. Rendering of fMRI results for each participant group. The statistical maps show the results of the voxel-wise comparison 'false memory rejection' > 'correct rejection of new word'. For depiction purposes results are shown at $P = 0.01$.

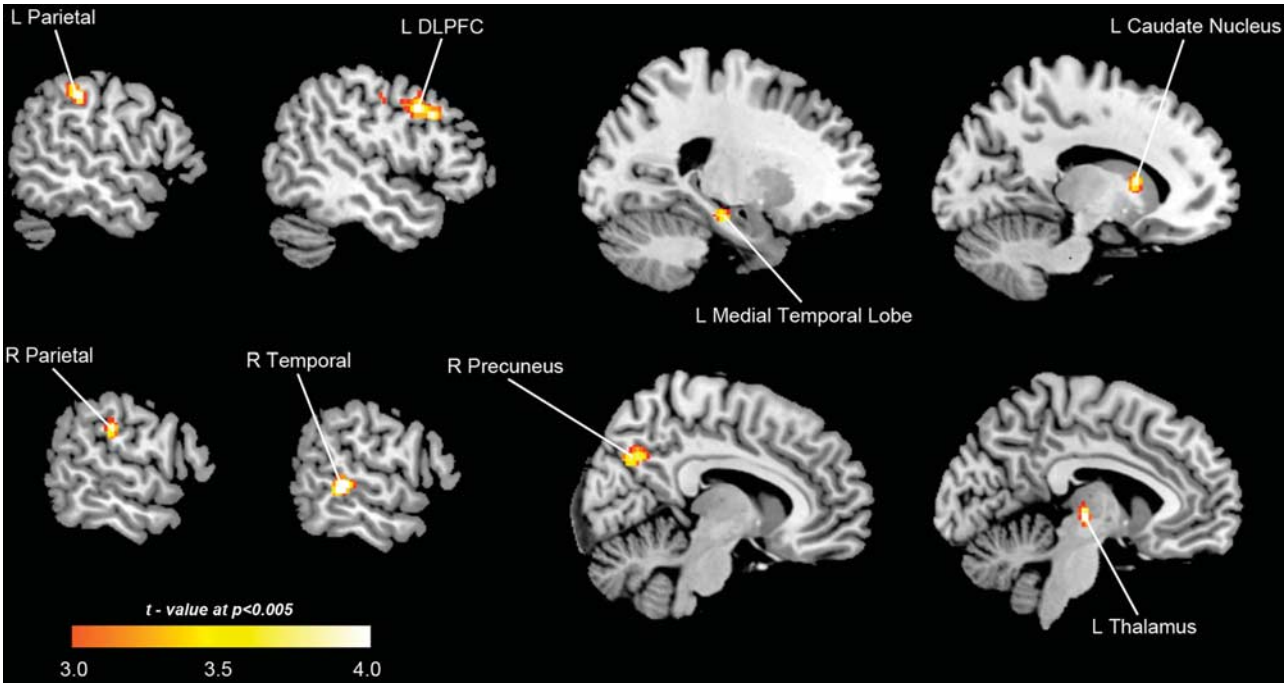

Figure 3. Group differences between controls and cannabis users. The images show the results of the voxel-wise independent-samples *t*-test controls > cannabis users for the contrast 'false memory rejection' > 'correct rejection of new word'. The brain regions depicted showed significantly higher activation in the control group as compared with the cannabis using group at $P = 0.001$ uncorrected. No significant results were obtained for the contrast cannabis users > controls. For depiction purposes results are shown at $P = 0.005$.

stored information. Cannabis users may have been left more dependent on the verbatim features of stimuli to decide whether a given word was a legitimate memory or not. Paradoxically, the greater activation of gist-related information in the control group compared with the cannabis group might have made them more vulnerable to false memories. Concurrent retrieval of item-based (verbatim) and context-based (gist) information in the control group might elicit conflict and require the engagement of cognitive control mechanisms, explaining the increased frontal activation observed in the controls. Thus, a more efficient conflict- or activation-monitoring, as signaled by increased dorsolateral prefrontal activity, may have led to the final outcome of better performance in the control group.

Further evidence of MTL and prefrontal impairment by cannabis is provided by magnetic resonance spectroscopy studies. Using this technique, researchers have found detrimental neurometabolic changes in these brain areas. For instance, Silveri and colleagues have reported decreased myo-inositol/creatine levels in the MTL and thalamus of users.[40,41] Hermann *et al.*[42] have found reduced *N*-acetyl-aspartate/total creatine ratios in the dorsolateral prefrontal of recreational users, and Cowan *et al.*[43] have found analogous decreases in Brodmann area 45 in the inferior frontal

Table 1. Areas of increased BOLD response in controls relative to cannabis users for the contrast: 'false memory rejection' > 'correct rejection of new word'

Brain region	*Lateralization*	*BA*	*MNI (x, y, z)*	*Maximum* t	n *voxels*
Temporal cortex	Right	22	60, −34, 2	5.14	64
Dorsolateral prefrontal	Left	9	−52, 16, 34	5.06	76
Red nucleus/thalamus	Left	–	−6, −18, −2	4.76	24
Parietal cortex	Left	40	-56, −32, 42	4.66	71
Parietal cortex	Right	40	60, −26, 28	4.03	15
Caudate	Left	–	−14, 12, 10	3.90	20
Medial temporal lobe	Left	35/28	−22, −22, −16	3.87	17
Precuneus	Right	7	10, −70, 32	3.82	23

Abbreviations: BA, Brodmann area; BOLD, blood oxygenation level dependent; MNI, coordinates in Montreal Neurological Institute stereotactic space; *t, t*-value (df = 30).

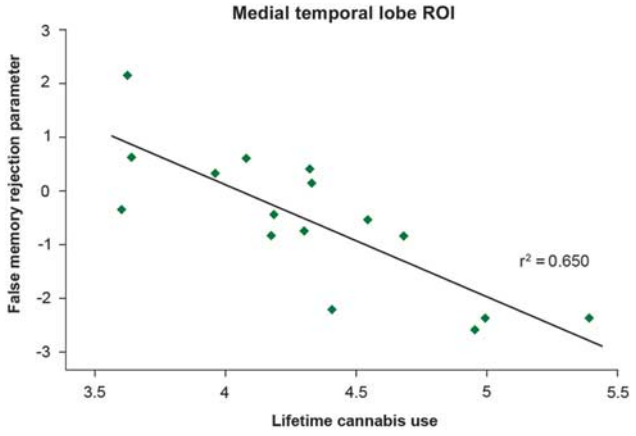

Figure 4. Correlation between MTL activity and cannabis exposure. The scatter plot shows the relationship between the individual statistical parameters in the MTL (beta values) associated with the 'false memory rejection' condition and lifetime cannabis use (log of estimated total number of cannabis cigarettes).

gyrus. Considering that analogous neurometabolic changes can be observed in older individuals[44] and that reality monitoring deficits increase with age,[45] we speculate that chronic cannabis use could aggravate the memory deficits associated with the normal ageing process.

Our findings extend previous knowledge on the impact of cannabis use on memory[12] and executive function.[8] Although there are contradictory results regarding the normalization of memory in the long term,[9,10,16] impairment has been associated with the intensity of cannabis use, with heavy users showing deficits in various memory functions.[46] Interestingly, many neuroimaging studies implementing simple memory tasks have failed to find differences in performance between heavy cannabis users and controls.[12] Our findings suggest that impairment may be more subtle and affect more complex cognitive processes, like those involved in the Deese-Roediger-McDermott paradigm.

A limitation of our study is the potential presence of residual THC levels in the brain in the absence of detectable levels in other biological matrices (in our case, urine). Whereas most studies in humans consider that cognitive testing after a 4-week period will assess the long-term effects of cannabis rather than its residual effects,[8] a longer persistence of THC in the brain has also been observed.[47] Thus, although unlikely, the presence of small amounts of THC in the body cannot be entirely ruled out.

Taken together, the present results indicate that long-term heavy cannabis users are at an increased risk of experiencing memory errors even when abstinent and drug-free. These deficits show a neural basis and suggest a subtle compromise of brain mechanisms involved in reality monitoring. Though subtle, the deficits found bear similarities with alterations observed in psychiatric and neurologic conditions and also with age-related cognitive decline. This lingering diminished ability to tell true from false may have medical, and legal implications. Future studies should address these issues and assess whether the deficits found here extend to other forms of memory distortion and reality monitoring beyond the false memory phenomenon.

CONFLICT OF INTEREST

The authors declare no conflict of interest.

ACKNOWLEDGMENTS

This work was supported by a grant from the 'Plan Nacional Sobre Drogas' of the Spanish Government. Marta Valle is supported by the 'Fondo de Investigación Sanitaria' through grant CP04/00121 from the Spanish Ministry of Health in collaboration with Institut de Recerca de l'Hospital de la Santa Creu i Sant Pau, Barcelona. Frederic Sampedro is supported by an FPU grant from the Spanish government. The authors wish to thank José Carlos Bouso for his help during participant recruitment and data collection, and Cesar Garrido and Núria Bargalló for technical assistance.

REFERENCES

1 United Nations Office on Drugs and Crime. World Drug Report 2014 2014; http://www.unodc.org/wdr2014/ (accessed 9 Mar2014).
2 Substance Abuse and Mental Health Services Administration. The NSDUH Report: Substance Use and Mental Health Estimates from the 2013 National Survey on Drug Use and Health: Overview of Findings 2014.
3 Wade L. South America. Legal highs make Uruguay a beacon for marijuana research. *Science* 2014; **344**: 1217.
4 Volkow ND, Baler RD, Compton WM. Weiss SRB. Adverse Health Effects of Marijuana Use. *N Engl J Med* 2014; **370**: 2219–2227.
5 Lopez-Quintero C, Pérez de los Cobos J, Hasin DS, Okuda M, Wang S, Grant BF *et al.* Probability and predictors of transition from first use to dependence on nicotine, alcohol, cannabis, and cocaine: results of the National Epidemiologic Survey on Alcohol and Related Conditions (NESARC). *Drug Alcohol Depend* 2011; **115**: 120–130.
6 Patton GC, Coffey C, Carlin JB, Degenhardt L, Lynskey M, Hall W. Cannabis use and mental health in young people: cohort study. *BMJ* 2002; **325**: 1195–1198.
7 Caspi A, Moffitt TE, Cannon M, McClay J, Murray R, Harrington H *et al.* Moderation of the effect of adolescent-onset cannabis use on adult psychosis by a functional polymorphism in the catechol-O-methyltransferase gene: longitudinal evidence of a gene X environment interaction. *Biol Psychiatry* 2005; **57**: 1117–1127.
8 Crean RD, Crane NA, Mason BJ. An evidence based review of acute and long-term effects of cannabis use on executive cognitive functions. *J Addict Med* 2011; **5**: 1–8.
9 Meier MH, Caspi A, Ambler A, Harrington H, Houts R, Keefe RSE *et al.* Persistent cannabis users show neuropsychological decline from childhood to midlife. *Proc Natl Acad Sci USA* 2012; **109**: E2657–E2664.
10 Solowij N, Battisti R. The chronic effects of cannabis on memory in humans: a review. *Curr Drug Abuse Rev* 2008; **1**: 81–98.

11 Solowij N, Jones KA, Rozman ME, Davis SM, Ciarrochi J, Heaven PCL *et al.* Verbal learning and memory in adolescent cannabis users, alcohol users and non-users. *Psychopharmacology (Berl)* 2011; **216**: 131–144.
12 Schoeler T, Bhattacharyya S. The effect of cannabis use on memory function: an update. *Subst Abuse Rehabil* 2013; **4**: 11–27.
13 Ranganathan M, D'Souza DC. The acute effects of cannabinoids on memory in humans: a review. *Psychopharmacology (Berl)* 2006; **188**: 425–444.
14 Curran HV, Brignell C, Fletcher S, Middleton P, Henry J. Cognitive and subjective dose-response effects of acute oral Delta 9-tetrahydrocannabinol (THC) in infrequent cannabis users. *Psychopharmacology (Berl)* 2002; **164**: 61–70.
15 Englund A, Morrison PD, Nottage J, Hague D, Kane F, Bonaccorso S *et al.* Cannabidiol inhibits THC-elicited paranoid symptoms and hippocampal-dependent memory impairment. *J Psychopharmacol* 2013; **27**: 19–27.
16 Pope HG, Gruber AJ, Hudson JI, Huestis MA, Yurgelun-Todd D. Neuropsychological performance in long-term cannabis users. *Arch Gen Psychiatry* 2001; **58**: 909–915.
17 Pope HG, Gruber AJ, Hudson JI, Huestis MA, Yurgelun-Todd D. Cognitive measures in long-term cannabis users. *J Clin Pharmacol* 2002; **42**: 41S–47S.
18 Ashtari M, Avants B, Cyckowski L, Cervellione KL, Roofeh D, Cook P *et al.* Medial temporal structures and memory functions in adolescents with heavy cannabis use. *J Psychiatr Res* 2011; **45**: 1055–1066.
19 Cousijn J, Wiers RW, Ridderinkhof KR, van den Brink W, Veltman DJ, Goudriaan AE. Grey matter alterations associated with cannabis use: results of a VBM study in heavy cannabis users and healthy controls. *Neuroimage* 2012; **59**: 3845–3851.
20 Yücel M, Solowij N, Respondek C, Whittle S, Fornito A, Pantelis C *et al.* Regional brain abnormalities associated with long-term heavy cannabis use. *Arch Gen Psychiatry* 2008; **65**: 694–701.
21 Kopelman MD. Varieties of false memory. *Cogn Neuropsychol* 1999; **16**: 197–214.
22 Schacter DL. The seven sins of memory. Insights from psychology and cognitive neuroscience. *Am Psychol* 1999; **54**: 182–203.
23 Dennis NA, Bowman CR, Peterson KM. Age-related differences in the neural correlates mediating false recollection. *Neurobiol Aging* 2014; **35**: 395–407.
24 Fuentemilla L, Càmara E, Münte TF, Krämer UM, Cunillera T, Marco-Pallarés J *et al.* Individual differences in true and false memory retrieval are related to white matter brain microstructure. *J Neurosci* 2009; **29**: 8698–8703.
25 Roediger HL, McDermott KB. Creating false memories: remembering words not presented in lists. *J Exp Psychol Learn Mem Cogn* 1995; **24**: 803–814.
26 Cabeza R, Rao SM, Wagner AD, Mayer AR, Schacter DL. Can medial temporal lobe regions distinguish true from false? An event-related functional MRI study of veridical and illusory recognition memory. *Proc Natl Acad Sci USA* 2001; **98**: 4805–4810.
27 Nelson HE, O'Connell A. Dementia: the estimation of premorbid intelligence levels using the New Adult Reading Test. *Cortex* 1978; **14**: 234–244.
28 Del Ser T, González-Montalvo JI, Martínez-Espinosa S, Delgado-Villapalos C, Bermejo F. Estimation of premorbid intelligence in Spanish people with the Word Accentuation Test and its application to the diagnosis of dementia. *Brain Cogn* 1997; **33**: 343–356.
29 Wechsler D. *Wechsler Adult Intelligence Scale-III (WAIS-III)*. The Psychological Corporation: San Antonio, TX, USA, 1981.
30 Binder JR, Desai RH, Graves WW, Conant LL. Where is the semantic system? A critical review and meta-analysis of 120 functional neuroimaging studies. *Cereb Cortex* 2009; **19**: 2767–2796.
31 Sheldon S, Moscovitch M. The nature and time-course of medial temporal lobe contributions to semantic retrieval: an fMRI study on verbal fluency. *Hippocampus* 2012; **22**: 1451–1466.
32 Ritchey M, Wing EA, LaBar KS, Cabeza R. Neural similarity between encoding and retrieval is related to memory via hippocampal interactions. *Cereb Cortex* 2013; **23**: 2818–2828.
33 Schacter DL, Slotnick SD. The cognitive neuroscience of memory distortion. *Neuron* 2004; **44**: 149–160.
34 McDermott KB, Jones TC, Petersen SE, Lageman SK, Roediger HL. Retrieval success is accompanied by enhanced activation in anterior prefrontal cortex during recognition memory: an event-related fMRI study. *J Cogn Neurosci* 2000; **12**: 965–976.
35 Parkin AJ, Bindschaedler C, Harsent L, Metzler C. Pathological false alarm rates following damage to the left frontal cortex. *Brain Cogn* 1996; **32**: 14–27.
36 Brainerd CJ, Reyna VF. Fuzzy-trace theory and false memory. *Curr Dir Psychol Sci* 2002; **11**: 164–169.
37 Balota DA, Cortese MJ, Duchek JM, Adams D, Roediger HL, McDermott KB *et al.* Veridical and false memories in healthy older adults and in dementia of the Alzheimer's type. *Cogn Neuropsychol* 1999; **16**: 361–384.
38 Ridderinkhof KR, Ullsperger M, Crone EA, Nieuwenhuis S. The role of the medial frontal cortex in cognitive control. *Science* 2004; **306**: 443–447.
39 Petrides M. Lateral prefrontal cortex: architectonic and functional organization. *Philos Trans R Soc B Biol Sci* 2005; **360**: 781–795.
40 Mashhoon Y, Jensen JE, Sneider JT, Yurgelun-Todd DA, Silveri MM. Lower Left Thalamic Myo-Inositol. Levels Associated with Greater Cognitive Impulsivity in Marijuana-Dependent Young Men: Preliminary Spectroscopic Evidence at 4T. *J Addict Res Ther* 2013; doi: 10.4172/2155-6105.S4-009.
41 Silveri MM, Jensen JE, Rosso IM, Sneider JT, Yurgelun-Todd DA. Preliminary evidence for white matter metabolite differences in marijuana-dependent young men using 2D J-resolved magnetic resonance spectroscopic imaging at 4 Tesla. *Psychiatry Res* 2011; **191**: 201–211.
42 Hermann D, Sartorius A, Welzel H, Walter S, Skopp G, Ende G *et al.* Dorsolateral prefrontal cortex N-acetylaspartate/total creatine (NAA/tCr) loss in male recreational cannabis users. *Biol Psychiatry* 2007; **61**: 1281–1289.
43 Cowan RL, Joers JM, Dietrich MS. N-acetylaspartate (NAA) correlates inversely with cannabis use in a frontal language processing region of neocortex in MDMA (Ecstasy) polydrug users: a 3T magnetic resonance spectroscopy study. *Pharmacol Biochem Behav* 2009; **92**: 105–110.
44 Fukuzako H, Hashiguchi T, Sakamoto Y, Okamura H, Doi W, Takenouchi K *et al.* Metabolite changes with age measured by proton magnetic resonance spectroscopy in normal subjects. *Psychiatry Clin Neurosci* 1997; **51**: 261–263.
45 McDaniel MA, Lyle KB, Butler KM, Dornburg CC. Age-related deficits in reality monitoring of action memories. *Psychol Aging* 2008; **23**: 646–656.
46 Bolla KI, Brown K, Eldreth D, Tate K, Cadet JL. Dose-related neurocognitive effects of marijuana use. *Neurology* 2002; **59**: 1337–1343.
47 Mura P, Kintz P, Dumestre V, Raul S, Hauet T. THC can be detected in brain while absent in blood. *J Anal Toxicol* 2005; **29**: 842–843.

Supplementary Information accompanies the paper on the Molecular Psychiatry website (http://www.nature.com/mp)